Photon diffractive dissociation in deep-inelastic scattering

E. Levin*
Fermilab, P.O. Box 500, Batavia, Illinois 60510

M. Wüsthoff
II. Institut für Theoretische Physik, Universität Hamburg, Germany
(Received 21 December 1992; revised manuscript received 25 April 1994)

This paper is mainly devoted to the presentation and discussion of formulas for the cross section of photon diffractive dissociation. The calculations which we present in a very detailed way are based on perturbative QCD. We improve formulas which describe this process in the triple Regge limit where the square of the missing mass M_X (the invariant mass of the bunch of secondary hadrons) is much larger than $|Q^2|$ and extend the range of validity to the region where M_X^2 is of the same order as $|Q^2|$. We introduce a diffractive dissociation structure function and show that it obeys the Gribov-Lipatov-Altarelli-Parisi evolution equation, but, with an additional inhomogeneous term. The relation to the Pomeron structure function is discussed.

PACS number(s): 13.60.Hb, 12.38.Bx, 12.40.Nn, 13.85.Qk

I. INTRODUCTION

Diffraction dissociation processes in general provides us with the basic information on the dynamics of "soft" interaction. In the framework of the old-fashioned Reggeon approach the soft interaction at high energies was reduced to the interaction between Pomerons via the triple Pomeron coupling constant (G_{3P} see Fig. 1). Its value was extracted from experimental data on diffractive dissociation with a large missing mass (invariant mass of the bunch of secondary hadrons M_X) [1,2] (see Fig. 1). Although there are large uncertainties in the value of G_{3P} (see [2]) the process of diffractive dissociation gives the only possibility to estimate this value.

The process of diffractive dissociation in deep-inelastic scattering looks especially interesting for three reasons.

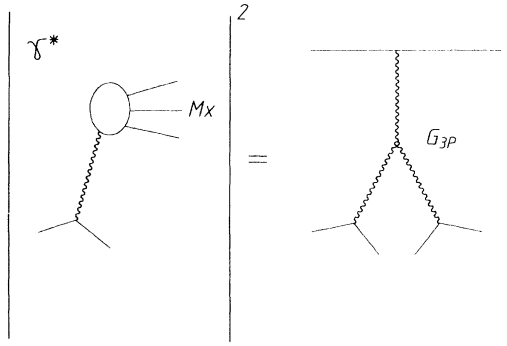

FIG. 1. Relation between diffractive dissociation and triple Pomeron diagram.

(1) The natural scale of hardness, namely, the large value of $|Q^2|$ (see Fig. 2) gives hope to develop the theoretical approach to this process within perturbative QCD. Such an approach was suggested in the paper of Gribov, Levin, and Ryskin (GLR) [3] and has been developed in a series of recent papers [4–6].

(2) The virtual photon in the diffractive dissociation probes the structure of the Pomeron. This means that this process could lead to a better understanding of the Pomeron structure. The idea to describe the diffractive dissociation process with the help of a Pomeron structure function was first introduced by Ingelman and Schlein [7] and has been discussed from another point of view in [8–11]. The perturbative approach to the diffractive dissociation allows to examine the above ideas on a theoretical basis and helps to clarify what the Pomeron structure is.

(3) The diffractive dissociation in deep-inelastic scattering is closely related to the screening (shadowing) corrections in deep-inelastic scattering through the Abramovski, Gribov, and Kancheli (AGK) cutting rules [12] as was noted in [3]. So diffractive dissociation can give direct information on the screening (shadowing) corrections, and the theoretical understanding of their nature is equivalent to the understanding of the nature of the screening (shadowing) corrections. Moreover, exper-

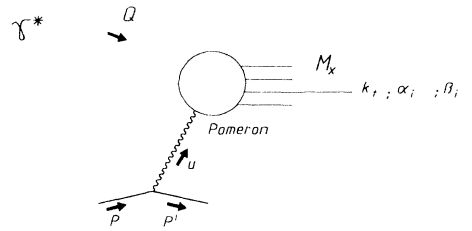

FIG. 2. Diffractive dissociation with Pomeron exchange.

*On leave from St. Petersbourg Nuclear Physics Institute, 188350 Gatchina, Russia.

imental studies of diffractive dissociation will test our understanding of screening corrections in the most direct way.

The main goal of this paper is to develop the leading log approximation (LLA) of the diffractive dissociation of the virtual photon in the framework of perturbative QCD and to present reliable formulas for this process. We hope that this paper provides a basis for the interpretation of DESY HERA's experimental data.

The paper is organized in the following way. In Sec. II, we discuss the kinematics, the small parameters, and the main results which include the evolution equation of the process and some comparison of the idea of the Pomeron structure function with our QCD approach. Section III contains the Born approximation of the production of two quarks, i.e., quark and antiquark, and the production of two quarks with an additional gluon (three-jet event). Section IV deals with the problem how to generalize to an infinite number of jets. In Sec. V we summarize our results, and the Appendixes contain all technical details of the calculations.

II. THE STRATEGY OF THE APPROACH AND THE MAIN RESULTS

A. Kinematics and notations

In this section we would like to outline our approach and we begin with the kinematics and the notations that we are going to use throughout the paper. First of all we would like to introduce the light-cone vector Q'_μ which characterizes the incoming virtual photon:

$$Q'_\mu = Q_\mu + x p_\mu \,, \tag{2.1}$$

where

$$x = \frac{|Q^2|}{2(Q,p)} \tag{2.2}$$

is the usual Bjorken variable. The main property of Q'_μ is the fact that

$$Q'^2 = Q^2 + 2x(Q,p) = 0 \,. \tag{2.3}$$

As energy variable we use

$$s = 2(Q,p) \,. \tag{2.4}$$

It is easy to see that

$$\bar{s} \equiv (Q+p)^2 = (1-x)s \,. \tag{2.5}$$

We expand all the momenta of the particles in our reaction in terms of Q'_μ and p_μ using Sudakov variables [13]. As example we take the momentum u which is transferred along the Pomeron and write it as

$$u_\mu = \alpha_u Q'_\mu + \beta_u p + u_{t\mu} \,. \tag{2.6}$$

Using Eq. (2.6) we can express the mass of the produced particles M_X^2 through α_u and β_u in the following way:

$$M_X^2 = (Q+u)^2 = (1+\alpha_u)(\beta_u - x)s + u_t^2 \tag{2.7}$$

while

$$(p-u)^2 = m^2 \;\text{ or }\; \alpha_u s - u_t^2 \approx 0 \,. \tag{2.8}$$

From Eqs. (2.7) and (2.8) we get

$$\begin{aligned} \beta_u &= \frac{M_X^2 + xs - u_t^2}{(1+\alpha_u)s} \\ &\approx \frac{M_X^2 + xs - u_t^2}{s} \\ &\approx \frac{M_X^2 + |Q^2|}{s} \end{aligned} \tag{2.9}$$

since $|\alpha_u| = u_t^2/s \ll 1$.

An important assumption for the diffractive dissociation process is the smallness of the missing mass M_X compared to the total energy $\sqrt{\bar{s}} \approx \sqrt{s}$. This means that [see Eq. (2.9)]

$$\beta_u - x \ll 1 \,. \tag{2.10}$$

B. The scale of hardness

If we want to apply perturbative QCD to the diffractive dissociation process, we need to specify the scale of hardness that appears in this process. Our first and natural scale is the large value of $|Q|^2$. But, this scale is not enough to apply the method of perturbative QCD. We need to specify what the Pomeron in QCD is. Our present understanding of the Pomeron in QCD could be expressed in the following way: the Pomeron is a ladder diagram (see Fig. 3). This approach can be justified only, if we assume that the initial virtuality $|Q_0^2|$ is sufficiently large and the final virtuality $|\bar{Q}_0^2|$ lies far above the initial one, namely,

$$|\bar{Q}_0^2| \gg |Q_0^2| \;\text{ and }\; \alpha_s(|Q_0^2|) \ll 1 \,. \tag{2.11}$$

It has to be stressed that we have to introduce both parameters Q_0 and $\bar{Q}_0$ *ad hoc*. Indeed, $|Q_0^2|$ (transverse momentum of the parton inside the proton) is the starting value for the GLAP-evolution equation [14]. If we know the proton structure function at $|Q_0^2|$, the GLAP-evolution equation gives the structure function at the larger scale $|Q^2|$. However, in the diffractive dissociation only partons with transverse momenta substan-

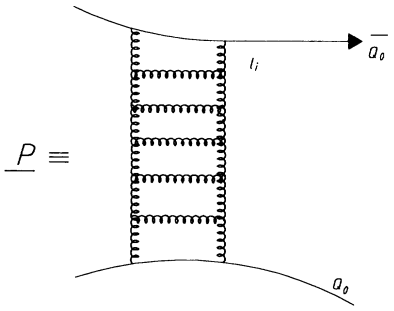

FIG. 3. The Pomeron as QCD ladder.

tially smaller than $|Q^2|$ are involved. In order to treat this case we need to assume that the minimal transverse momentum of the produced particles is large enough ($|k_{i_t}| \geq |\bar{Q}_0|$) to be sure that perturbative QCD still works while calculating the cross section. A negative consequence is that we cannot calculate the total cross section of diffractive dissociation. What we actually do is to calculate a part of the diffractive dissociation, namely, the cross section of the following process:

$$\gamma^*(Q^2) + p \to \text{jets}(|k_{t_{\text{jet}}}| \geq |\bar{Q}_0|) + X + p' \,. \tag{2.12}$$

The kinematical restriction could be imposed by an experiment which measures only hard jets, i.e., jets with a transverse momentum larger than some scale $|\bar{Q}_0^2|$. The formula that we are going to calculate covers the hard part of the cross section. The question then is, how far can we extrapolate our results towards smaller values of $|\bar{Q}_0^2|$. For this case we have to compare our formula with the soft Pomeron phenomenology. This will be done in some later publication. In this paper we will discuss special kinematical regions of β_u and x-Bjorken where a lower cutoff in our integration becomes unnecessary. $|\bar{Q}_0^2|$ then takes some natural value.

C. Small parameters and leading logs of the approach

In this subsection we would like to clarify what our small parameters are and which type of logs we are able to sum in LLA of QCD. We first have a look at the double leading log approximation (DLA). This approximation was used in earlier calculations of diffractive dissociation [3,5]. It is capable to explain the most typical and important features of this process. In our paper we concentrate on the generalization to the case of single leading log approximation.

Now let us list the parameters for DLA:

$$\alpha_s \ln\frac{\beta_u}{x} \leq 1, \quad \alpha_s \ln\frac{Q^2}{\bar{Q}_0^2} \leq 1 \,,$$

$$\alpha_s(|\bar{Q}_0^2|) \ll 1 \,, \tag{2.13}$$

$$\alpha_s \ln\frac{\beta_u}{x} \ln\frac{Q^2}{\bar{Q}_0^2} \geq 1 \,,$$

and

$$\alpha_s \ln\frac{1}{\beta_u} \leq 1, \quad \alpha_s \ln\frac{\bar{Q}_0^2}{Q_0^2} \leq 1 \,,$$

$$\alpha_s(|Q_0^2|) \ll 1 \,, \tag{2.14}$$

$$\alpha_s \ln\frac{1}{\beta_u} \ln\frac{\bar{Q}_0^2}{Q_0^2} \geq 1 \,.$$

Using these small parameters we are able to calculate the cross section of the process shown in Eq. (2.12) in the kinematical region:

$$1 \gg \beta_u \gg x \,,$$

$$|Q^2| \gg |\bar{Q}_0^2| \gg |Q_0^2| \,, \tag{2.15}$$

$$|u_t^2| \ll |Q_0^2| \,.$$

The set of parameters in Eqs. (2.13) and (2.14) indicates the kind of logs we take into account. It is clear from Fig. 4 that we sum all logs due to integration over β_i and k_{i_t} of the emitted protons ($\ln\frac{1}{\beta_i}\ln|k_{i_t}^2|$) while we calculate the structure of the Pomeron in DLA.

The most important property of the cross section for diffractive dissociation in comparison to the usual leading log approach of the deep-inelastic structure function is the higher twist integral over the transverse momentum of the slowest parton which has no logarithmic character and looks as follows (see also Fig. 4):

$$\int_{|\bar{Q}_0^2|}^{|Q^2|} \frac{d|k_t^2|}{k_t^4} \,. \tag{2.16}$$

This integral indicates the need of introducing the lower cutoff $|\bar{Q}_0^2|$ for $|k_t^2|$. If there were none, the integral above could dominate at the absolutely lowest bound $|Q_0^2|$, i.e., there would be no room for the Pomeron to evolve. We have to take care and introduce a new lower bound which lies sufficiently far above $|Q_0^2|$. Another point which is illustrated by expression (2.16) is the fact that, since

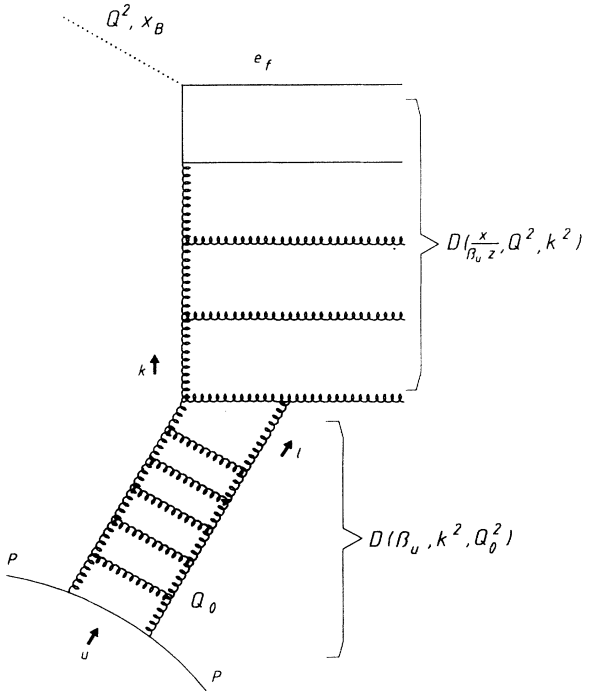

FIG. 4. The QCD model of the diffractive dissociation in the triple Regge limit.

QCD is a dimensionless theory, the extra dimension coming from the integration over the momentum transferred along the Pomeron (in our case the integral over u_t^2) is compensated by $\frac{1}{|k_t^2|}$. The extra power in the denominator of expression (2.16) also suggests the conclusion that the main contribution to the total cross section of reaction (2.12) originates from the region where $k_t \approx \bar{Q}_0$ and that we can neglect logs of the type $\ln k_t^2/\bar{Q}_0^2$.

We are going to improve our DLA approach by expanding it to the following kinematical region:

$$1 \gg \beta_u \geq x \,,$$
$$|Q^2| \gg |\bar{Q}_0^2| \gg |Q_0^2| \,, \tag{2.17}$$
$$|u_t^2| \ll |Q_0^2| \,.$$

In this region we sum all logs $\ln Q^2/\bar{Q}_0^2$ but $\alpha_s \ln \frac{x}{\beta_u} \ll 1$. This means that the energy (β_i in Fig. 2) of the produced particles may be uniformly distributed among them without any ordering.

D. The main properties of the answer

In this section we start the discussion of the final results for the cross section of reaction (2.12). The details of the calculation will be given in the next subsections.

The result is the generalized formula of GLR [3] now valid in the kinematical region (2.17) and looks as follows:[1]

$$\frac{\beta_u d\sigma^{DD}}{d\beta_u d|u_t^2|}(\gamma^* + p \to \text{jet}(|k_t| > |\bar{Q}_0|) + X + p')\Big|_{|u_t^2| \ll |Q_0^2|}$$
$$= |G_p^{2G}(|u_t^2|)|^2 \sum_F \frac{4\pi^2 e_F^2 \alpha_{\text{em}}}{|Q^2|} \int_{x/\beta_u}^1 \frac{dz}{z}\frac{x}{\beta_u} \int_{|\bar{Q}_0^2|}^{|Q^2|} \frac{d|k_t^2|}{k_t^4} \frac{\alpha_s^2(|k_t^2|)}{16}$$
$$\times \left[\Phi_P^F(z) D_F^F\left(\frac{x}{\beta_u z}, |Q^2|, |k_t^2|\right) + \Phi_P^G(z) D_G^F\left(\frac{x}{\beta_u z}, |Q^2|, |k_t^2|\right)\right] [\beta_u D_p^G(\beta_u, |k_t^2|, |Q_0^2|+)]^2 \,. \tag{2.18}$$

All notations should be clear from Fig. 4. G_p^{2G} denotes the proton form factor which is 1 for $u_t^2 = 0$. Any function D stands for the particle distribution of a dressed parton (quark or gluon) after evolution from some low to some large virtuality. In expression (2.18) we use as variable of integration the transverse momentum $|k_t^2|$ with its lower limit $|\bar{Q}_0^2|$. As the upper limit we take $|Q^2|$ which is usually the upper boundary of the virtuality and not the transverse momentum squared $|k_t^2|$, but, since we are not interested in the extreme infrared region $M_X \to 0$ we are allowed to do this. We just have to take care that $M_X^2 \gg 4C_F(\xi_Q - \xi_{\bar{Q}_0})\Lambda^2$ where ξ_m is defined as $\xi_m = \frac{1}{b}\ln\ln|m^2|/\Lambda^2$ for any momentum m and Λ denotes Λ_{QCD}. This restriction avoids the region where the LLA(Q^2) becomes invalid and the resummation of $\ln(n)$, the logarithm of the moments n, at large n becomes important. The main new results of Eq. (2.18) are the splitting functions Φ_P^F, Φ_P^G which were derived in [22] and which we will call Pomeron splitting functions. They describe the interaction of the Pomeron with quarks and gluons. New in comparison with the GLR formula is the Pomeron interaction with quarks. This process has been calculated in the [5,6] but with two different results. So we repeated the calculation in a slightly different technique and found the splitting function Φ_P^F which is the corrected version of [5] and which coincides with the result in [6]. Besides, we found the second splitting function Φ_P^G which describes the interaction of the Pomeron with gluons not only in the region of small z (triple Regge limit) but also for z of the order of 1. This means that we extended the region of applicability to the complete region including large missing masses (M_X) as well as small missing masses.

1. *Pomeron splitting functions*

The explicit expressions for the new splitting functions are

$$\Phi_P^F(z) = \frac{1}{2N} 16 z^2 (1-z)^2 \,,$$
$$\Phi_P^G(z) = \frac{2N^2}{N^2-1} 4z(1-z)^3 \left(2 + \frac{1}{z}\right)^2 \,. \tag{2.19}$$

Although we used the name "Pomeron splitting functions" in analogy to the Gribov-Lipatov-Altarelli-Parisi (GLAP) splitting functions, they do not have the same properties. This is obvious in the case of Φ_P^G which is

[1]For transverse polarized photons.

not symmetric under the interchange of z and $1-z$. The strong suppression in $1-z$ is due to color cancellation which effects the real emission of soft gluons from the colorless Pomeron. The virtual gluon, on the other hand, behaves different and still has the typical soft distribution $1/z$ in its longitudinal momentum fraction z. The asymptotic expression for small z was found before [5].

2. *The diffractive dissociation structure function and its evolution equation*

In order to find an evolution equation for our process it is convenient to introduce a new structure function which describes the contribution of diffractive dissociation to the general structure function of deep inelastic scattering. Namely,

$$D_{DD}^{F,G}\left(\frac{x}{\beta_u},\beta_u,|Q^2|,|\bar{Q}_0^2|,|Q_0^2|\right)=\int|G_P^{2G}(|u_t^2|)|^2 d|u_t^2|\int_{x/\beta_u}^1\frac{dz}{z}\int_{|\bar{Q}_0^2|}^{|Q^2|}\frac{d|k_t^2|}{k_t^4}\frac{\alpha_s^2(|k_t^2|)}{16}$$
$$\times\left[\Phi_P^F(z)D_F^{F,G}\left(\frac{x}{\beta_u z},|Q^2|,|k_t^2|\right)+\Phi_P^G(z)D_G^{F,G}\left(\frac{x}{\beta_u z},|Q^2|,|k_t^2|\right)\right]$$
$$\times[\beta_u D_P^G(\beta_u,|k^2|,|Q_0^2|)]^2\ . \tag{2.20}$$

Differentiating Eq. (2.20) with respect to $\ln(Q^2/\Lambda^2)$ leads to the following equations:

$$\frac{\partial}{\partial\ln\left(\frac{|Q^2|}{\Lambda^2}\right)}D_{DD}^{F,G}\left(\frac{x}{\beta_u},\beta_u,|Q^2|,|\bar{Q}_0^2|,|Q_0^2|\right)$$
$$=\frac{\alpha_s(|Q^2|)}{4\pi}\int_{x/\beta_u}^1\frac{dz}{z}$$
$$\times\left[\Phi_F^{F,G}(z)D_{DD}^F\left(\frac{x}{\beta_u z},\beta_u,|Q^2|,|\bar{Q}_0^2|\right)+\Phi_G^{F,G}(z)D_{DD}^G\left(\frac{x}{\beta_u z},\beta_u,|Q^2|,|\bar{Q}_0^2|\right)\right]$$
$$+\frac{\int|G_p^{2G}(|u_t^2|)|^2 d|u_t^2|}{|Q^2|}\frac{\alpha_s^2(|Q^2|)}{16}\Phi_P^{F,G}\left(\frac{x}{\beta_u}\right)[\beta_u D_p^G(\beta_u,|Q^2|,|Q_0^2|)]^2\ . \tag{2.21}$$

The functions Φ_F^F, Φ_F^G, Φ_G^F, and Φ_G^G are the usual splitting functions in the GLAP equation. The other splitting functions were defined in Eq. (2.19). The initial condition at $|k_t^2|=|\bar{Q}_0^2|$ for $D_{DD}^{F,G}$ is zero as can be seen from Eq. (2.18).

We would like to discuss now the possibility of introducing a Pomeron structure function following the idea of Ingelman and Schlein [7], which is simply the solution of the usual GLAP-evolution equation with new initial conditions. Looking at Eq. (2.21) it seems to be impossible to introduce something like the structure function of the Pomeron. This becomes clear even by looking at Eq. (2.20), since the structure function that corresponds to the Pomeron exchange ($\beta_u D_p^G$) explicitly depends on $|k_t^2|$ and cannot be replaced by the flux of the Pomeron as it was done in Ref. [7]. However, in the region of not extremely small β_u (see point 5) when the value of $(\beta_u D_p^G)^2$ cannot compensate the factor $\frac{1}{k_t^4}$ in the integral, we can see that the integration over $|k_t^2|$ is concentrated at $|k_t^2|\approx|\bar{Q}_0^2|$. Moreover, $|Q^2|$ should be much larger than $|\bar{Q}_0^2|$. In this kinematical region we can replace $\beta_u D_p^G(\beta_u,|k_t^2|,|Q_0^2|)$ by $\beta_u D_p^G(\beta_u,|\bar{Q}_0^2|,|Q_0^2|)$ and define the Pomeron structure function through its initial condition at $|Q^2|=|\bar{Q}_0^2|$:

$$D_P^{F,G}\left(\frac{x}{\beta_u},|\bar{Q}_0^2|,|\bar{Q}_0^2|\right)=\frac{1}{\frac{93}{20}+\frac{4n_F}{45}}\Phi_P^{F,G}\left(\frac{x}{\beta_u}\right)\ , \tag{2.22}$$

where n_F denotes the number of flavors. We have normalized the Pomeron structure function with respect to the energy sum rule:

$$\int_0^1 dzz\left[\sum_F D_P^F(z,|Q^2|,|\bar{Q}_0^2|)+D_P^G(z,|Q^2|,|\bar{Q}_0^2|)\right]=1\ . \tag{2.23}$$

The corresponding GLAP evolution equation reads

$$\frac{\partial}{\partial\ln\left(\frac{|Q^2|}{\Lambda^2}\right)}D_P^{F,G}\left(\frac{x}{\beta_u},|Q^2|,|\bar{Q}_0^2|\right)=\frac{\alpha_s(|Q^2|)}{4\pi}\int_{\frac{x}{\beta_u}}^1\frac{dz}{z}\left[\Phi_F^F(z)D_P^F\left(\frac{x}{\beta_u z},|Q^2|,|\bar{Q}_0^2|\right)+\Phi_G^F(z)D_P^G\left(\frac{x}{\beta_u z},|Q^2|,|\bar{Q}_0^2|\right)\right]\ . \tag{2.24}$$

Since we introduced the normalized Pomeron structure function, we have to absorb all remaining factors into the Pomeron flux factors:[2]

[2]We would like to thank Ingelman who has provided us with the idea of an additional flux factor.

$$f_P(\beta_u,|\bar{Q}_0^2|,|Q_0^2|)=\left(\frac{93}{20}+\frac{4n_F}{45}\right)\frac{\int du_t^2|G_p^{2G}(|u_t^2|)|^2}{|\bar{Q}_0^2|}\frac{\alpha_s^2(|\bar{Q}_0^2|)}{16}[\beta_u D_p^G(\beta_u,|\bar{Q}_0^2|,|Q_0^2|)]^2$$
$$\simeq\left(\frac{93}{20}+\frac{4n_F}{45}\right)\frac{|Q_0^2|}{|\bar{Q}_0^2|}\frac{\alpha_s^2(|\bar{Q}_0^2|)}{16}[\beta_u D_p^G(\beta_u,|\bar{Q}_0^2|,|Q_0^2|)]^2\,. \tag{2.25}$$

The relation between Pomeron structure function and diffractive dissociation structure function is

$$D_{DD}^{F,G}\left(\frac{x}{\beta_u},\beta_u,|Q^2|,|\bar{Q}_0^2|,|Q_0^2|\right)=f_P(\beta_u,|\bar{Q}_0^2|,|Q_0^2|)D_P^{F,G}\left(\frac{x}{\beta_u},|Q^2|,|\bar{Q}_0^2|\right)\,. \tag{2.26}$$

We see that factorization approximately holds. How good it works has to be checked numerically, but it seems to be advisable to use this approach for a first analysis of DESY HERA's data. One more interesting remark concerns the momentum fraction carried by gluons and quarks inside the Pomeron. It turns out that the gluon fraction roughly makes up $(100\text{–}1.9n_F)\%$ of the total momentum which suggests a strong gluon dominance.

If we want to evaluate the total cross section of diffractive dissociation including the soft region at small $|k_t|$, we have to move to the "soft" Pomeron phenomenology with the experimental value G_{3P}. At $|k_t|\approx\bar{Q}_0$ we can match our "hard" formulas with the phenomenological ones and extract the value of the natural cutoff $\bar{Q}_0$.

3. *Transverse momentum distribution of the slowest jet in the diffractive dissociation*

As was noted in [5] we have a different distribution over the transverse momentum of the slowest jet (k_t in Fig. 4) compared to the usual deep-inelastic events. It is easy to see directly from Eq. (2.18) that

$$\left.\frac{\beta_u d\sigma^{DD}}{d\beta_u d|u_t^2|d|k_t^2|}\right|_{|u_t^2|\ll|Q_0^2|}=|G_p^{2G}(|u_t^2|)|^2\sum_F\frac{4\pi^2e_F^2\alpha_{\rm em}}{|Q^2|}\frac{\alpha_s^2(|k_t^2|)}{16}\frac{1}{k_t^4}\int_{\frac{x}{\beta_u}}^1\frac{dz}{z}\frac{x}{\beta_u}$$
$$\times\left[\Phi_P^F(z)D_F^F\left(\frac{x}{\beta_u z},|Q^2|,|k_t^2|\right)+\Phi_P^G(z)D_G^F\left(\frac{x}{\beta_u z},|Q^2|,|k_t^2|\right)\right][\beta_u D_P^G(\beta_u,|k_t^2|,|Q_0^2|)]^2\,. \tag{2.27}$$

The main factor here is $\frac{1}{k_t^4}$ while the corresponding distribution in the deep-inelastic scattering is proportional to $\frac{1}{|k_t^2|}$. We see that in diffractive dissociation the typical transverse momentum is much smaller and the dependence on the lower cutoff much stronger than in the usual deep-inelastic scattering.

4. *Screening corrections (SC) versus diffractive dissociation*

Due to the AGK cutting rules [12] the diffractive process is intimately related to the screening corrections. The screening ΔF_2 can be understood as the deviation of the measured F_2 from the purely GLAP-evolved structure function $F_2^{\rm GLAP}$:

$$F_2(x,|Q^2|,|Q_0^2|)=F_2^{\rm GLAP}(x,|Q^2|,|Q_0^2|)+\Delta F_2(x,|Q^2|,|Q_0^2|)\,. \tag{2.28}$$

It is supplementary to the factorization theorem [15]. The AGK cutting rules say that

$$\Delta F_2(x,|Q^2|,|Q_0^2|)=-\lim_{|\bar{Q}_0^2|\to|Q_0^2|}\int_x^1 d\beta_u\frac{x}{\beta_u}D_{DD}^F\left(\frac{x}{\beta_u},\beta_u,|Q^2|,|\bar{Q}_0^2|\right)\,, \tag{2.29}$$

i.e., the screening corrections are negative and their absolute value identical to the integrated diffractive structure function. In other words, the sum of the cross sections of the total inclusive deep-inelastic scattering and the inclusive diffractive deep-inelastic scattering is free of the screening corrections and simply obeys the GLAP evolution equations. This relation may help to check the AGK cutting rules experimentally.

Another interesting quantity is the ratio R of the moments (n) of the integrated gluon diffractive structure function and the usual gluon-proton structure function

$$R(n,Q^2)=\frac{|\Delta F^G(n,Q^2)|}{F^G(n,Q^2)}\,, \tag{2.30}$$

where ΔF^G is defined in a similar way as ΔF_2:

$$|\Delta F^G(x,|Q^2|,|Q_0^2|) = \lim_{|\bar{Q}_0^2|\to|Q_0^2|} \int_x^1 d\beta_u \frac{x}{\beta_u} D_{DD}^G\left(\frac{x}{\beta_u},\beta_u,|Q^2|,|\bar{Q}_0^2|\right) . \tag{2.31}$$

The scaling violation of R is directly related to the inhomogeneous term of our evolution equation for diffractive dissociation (2.21):

$$\frac{\partial R(n,Q^2)}{\partial \ln\left(\frac{|Q^2|}{\Lambda^2}\right)} = \frac{\int |G_p^{2G}(|u_t^2|)|^2 d|u_t^2|}{|Q^2|} \frac{\alpha_s^2(|Q^2|)}{16} \frac{2N^2}{N^2-1} \frac{4}{n-1} \frac{\int_0^1 d\beta_u \beta_u^{n-1}[\beta_u D_p^G(\beta_u,|Q^2|,|Q_0^2|)]^2}{F^G(n,Q^2)} \left\{1+\frac{|\Delta F^G|}{F^G}\right\} . \tag{2.32}$$

R underlies a strong scaling violation $1/Q^2$. In the framework of a Pomeron structure function and the assumption of factorization [Eq. (2.26)] the scaling violation of R should be zero. For asymptotic large Q^2 this is true. So, measuring R will help to understand, whether diffractive dissociation can be described within the usual perturbative QCD in terms of a Pomeron structure function and whether the screening corrections are more than just some invisible renormalization of the initial structure function at some low scale $|Q_0^2|$.

5. *The triple Regge limit, $\beta_u \gg x$*

Taking our master equation (2.18) again, we would like to examine the region: $s \gg M_X^2 \gg |Q^2|$. We claim that in this region we do not need the lower cutoff $|\bar{Q}_0^2|$ and integrate over the complete region of $|k_t^2|$. This has already been discussed in the GLR paper [3], but here we are going to stress some particular features of diffractive dissociation (see also [5]).

In order to illustrate all problems and properties of our process let us use the double log asymptotics for all our structure functions in Eq. (2.18), namely,

$$xG(x,|Q^2|,|k^2|) \sim \exp\left\{\sqrt{16N(\xi_Q-\xi_k)\ln\left(\frac{1}{x}\right)}\right\} . \tag{2.33}$$

With this asymptotic expression the integral in (2.18) looks as follows:

$$\int_{\xi_{Q_0}}^{\xi_Q} d\xi_k \exp\left\{-2b\xi_k - e^{b\xi_k} + \sqrt{16N(\xi_Q-\xi_k)\ln\left(\frac{\beta_u}{x}\right)} + 2\sqrt{16N(\xi_k-\xi_{Q_0})\ln\left(\frac{1}{\beta_u}\right)}\right\} . \tag{2.34}$$

The z integration has only a small effect on the following analysis and we ignore it here. We search for a saddle-point solution of Eq. (2.34) and find that following equation which determines the value of our saddle point ξ_k^0:

$$be^{b\xi_k^0} + \frac{1}{2}\sqrt{16N\frac{\ln(\beta_u/x)}{\xi_Q-\xi_k^0}} - \sqrt{16N\frac{\ln(1/\beta_u)}{\xi_k^0-\xi_{Q_0}}} = 0 . \tag{2.35}$$

In the region

$$xi_k^0 \ll \frac{1}{2b}\ln\left[\frac{4N}{b^2}\frac{\ln\left(\frac{\beta_u}{x}\right)}{\xi_Q-\xi_k^0}\right] , \tag{2.36}$$

we can easily find the solution of Eq. (2.35), namely,

$$\xi_k^0 = \frac{4\ln\left(\frac{1}{\beta_u}\right)\xi_Q + \ln\left(\frac{\beta_u}{x}\right)\xi_{Q_0}}{4\ln\left(\frac{1}{\beta_u}\right)+\ln\left(\frac{\beta_u}{x}\right)} . \tag{2.37}$$

The kinematical region considered here corresponds to a missing mass squared M_X^2 which is much larger than $|Q^2|$. The upper ladder and the lower two ladders balance each other. The factor $\frac{1}{k_t^4}$ has a minor effect. The opposite kinematical region is

$$\xi_k^0 \gg \frac{1}{2b}\ln\left[\frac{4N}{b^2}\frac{\ln\left(\frac{\beta_u}{x}\right)}{\xi_Q-\xi_k^0}\right] . \tag{2.38}$$

Equation (2.35) then changes into

$$\xi_k^0 + \frac{1}{2b}\ln[b(\xi_k^0-\xi_{Q_0})] - \frac{1}{2b}\ln\left[\frac{16N}{b}\ln\left(\frac{1}{\beta_u}\right)\right] = 0 . \tag{2.39}$$

A further restriction

$$\frac{16N}{b^2}\ln\left(\frac{1}{\beta_u}\right) + \xi_{Q_0} \gg \xi_k^0 \gg \frac{1}{2b}\ln\left[\frac{4N}{b^2}\frac{\ln\left(\frac{\beta_u}{x}\right)}{\xi_Q-\xi_k^0}\right] \tag{2.40}$$

leads to the solution

$$\xi_k^0 = \frac{1}{2b}\ln\left[\frac{16N}{b}\ln\left(\frac{1}{\beta_u}\right)\right] . \tag{2.41}$$

In the region that we are discussing now, the missing mass M_X is either much smaller than $\sqrt{s}$ nor extremely large compared to $\sqrt{|Q^2|}$. In this case the two lower ladder are balanced by the factor $\frac{1}{k_t^4}$.

Both solutions show that we no longer need a lower cutoff $|\bar{Q}_0^2|$ for $|k_t^2|$, i.e., the cross section does not depend on $|\bar{Q}_0^2|$.

The second solution (2.41) has the advantage that it only depends on β_u and not on $|Q^2|$ so that factorization holds. The new sale $|k_0^2|$ [see Eq. (2.41)]

$$|k_0^2| = \Lambda^2 \exp\left[\sqrt{\frac{16N}{b}\ln\left(\frac{1}{\beta_u}\right)}\right] \tag{2.42}$$

serves as starting point for the evolution Eq. (2.24) where the flux factor, now, includes the width of the saddle:

$$D_{DD}^{F,G}\left(\frac{x}{\beta_u},\beta_u,|Q^2|\right) = f_P(\beta_u,|Q_0^2|)D_P^{F,G}\left(\frac{x}{\beta_u},\beta_u,|Q^2|\right), \tag{2.43}$$

$$f_P(\beta_u,|Q_0^2|) = \left(\frac{93}{20}+\frac{4n_F}{45}\right)\sqrt{2\pi}\left\{\left[1+\frac{1}{2(\xi_{k_0}-\xi_{Q_0})}\right]b^2\ln\left(\frac{|k_0^2|}{\Lambda^2}\right)\right\}^{-\frac{1}{2}}$$

$$\times\frac{\int|G_p^{2G}(|u_t^2|)|^2 d|u_t^2|}{|k_0^2|}\frac{\alpha_s^2(|k_0^2|)}{16}[\beta_u D_p^G(\beta_u,|k_0^2|,|Q_0^2|)]^2 .$$

So far we assumed the simple double leading log asymptotics for the proton structure function which has to be modified by taking into account shadowing (screening) corrections. These corrections correspond to diagrams shown in Fig. 5 which were summed by the nonlinear evolution equation (GLR equation, see [3,17]). Since the GLR equation only gives the possibility to calculate the structure function in the region where the shadowing corrections are still small, we need for very small β_u some additional hypothesis, the so-called parton density saturation hypothesis:

$$\beta_u D_p^G(\beta_u,|k^2|,|Q_0^2|) = \begin{cases} a\frac{|k^2|}{q_0^2(\beta_u)} & \text{for } |k^2| < q_0^2(\beta_u), \\ a\frac{q_0^2(\beta_u)}{|k^2|} & \text{for } |k^2| > q_0^2(\beta_u), \end{cases} \tag{2.44}$$

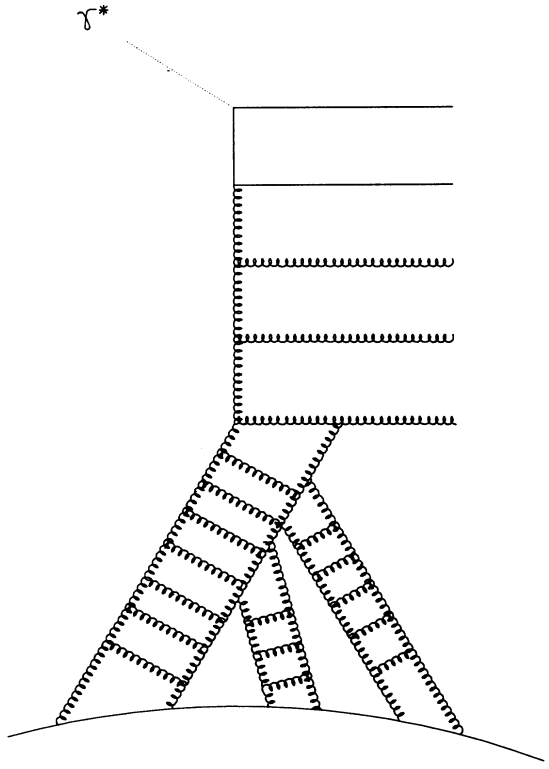

FIG. 5. Screening (shadowing) correction to the proton structure function.

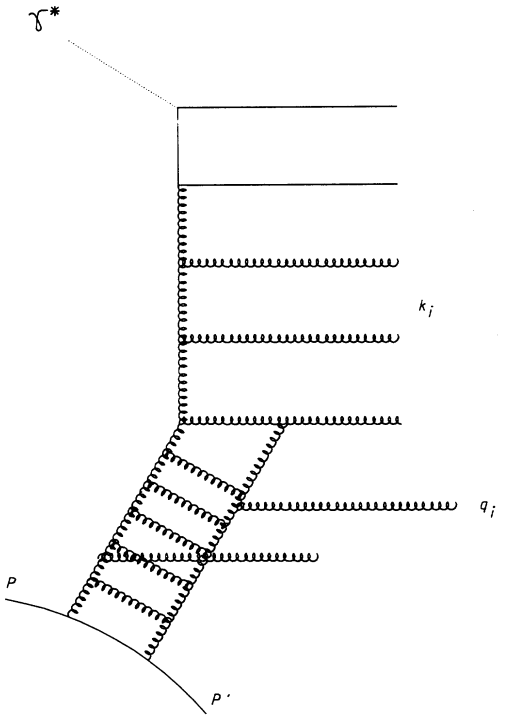

FIG. 6. Additional gluon production leading to logarithmic contribution below the cell with dk_t^2/k_t^4 integration.

where $q_0^2(\beta_u)$ is equal to (see [3,5])

$$q_0^2(\beta_u) = Q_0^2 + \Lambda^2 \exp\left\{3.56\sqrt{\ln\left(\frac{\beta_0}{\beta_u}\right)}\right\} . \quad (2.45)$$

In the framework of the saturation hypothesis we can calculate the total cross section of diffractive dissociation. It is easy to see that using Eq. (2.44) the integral over $|k_t^2|$ in Eq. (2.18) is convergent and takes the factorized form

$$\left.\frac{\beta_u d\sigma^{DD}}{d\beta_u d|u_t^2|}(\gamma^* p \to Xp')\right|_{|u_t^2|\ll|Q_0^2|} = |G_p^{2G}(|u_t^2|)|^2 \sum_F \frac{4\pi^2 e_F^2 \alpha_{\rm em}}{|Q^2|}\frac{4}{3}\frac{a^2}{q_0^2(\beta_u)}\int_{\frac{x}{\beta_u}}^1 \frac{dz}{z}\frac{x}{\beta_u}\frac{\alpha_s^2[q_0^2(\beta_u)]}{16}$$
$$\times\left[\Phi_P^F(z)D_F^F\left(\frac{x}{\beta_u z},|Q^2|,q_0^2(\beta_u)\right)+\Phi_P^G(z)D_G^F\left(\frac{x}{\beta_u z},|Q^2|,q_0^2(\beta_u)\right)\right] . \quad (2.46)$$

At the end of this section we would like to mention corrections that we have not taken into account. First of all we have neglected the Pomeron-Pomeron interaction (see Fig. 6) [19,18]. We think that due to the lower cutoff in $|k_t^2|$ and the color recoupling, which gives a factor $1/(N^2-1)$, this correction turns out to be negligible. A second type of correction comes from higher twist contributions, and we may have missed some important part of the phase space due to our strong ordering assumption. Our experience tells us that these corrections should be small, but they have to be studied in more detail.

III. PHOTON DIFFRACTION DISSOCIATION AT BORN LEVEL

This section is devoted to the technical details of the calculation of the diffractive dissociation cross section at Born level. The next section will include the generalization to higher order of perturbation theory.

Due to the fact that the photon couples to quarks only (and not to gluons) the minimal configuration of the diffractive dissociation process is the dissociation into two quark jets (quark and antiquark) (Fig. 7). The next step towards the complete description of photon diffractive dissociation is the inclusion of one gluon jet (Fig. 12). These two cases serve as starting point for the generalization.

A. Photon diffractive dissociation into two jets

Since photon diffractive dissociation is part of the general deep-inelastic scattering, another name for our process could be diffractive deep-inelastic scattering. New in the case of diffractive dissociation is the more exclusive final state which contains the proton only slightly scattered. The rest of the particles in the final state (here quark and antiquark) take the quantum numbers of the photon. The quarks and the proton are well separated in rapidity provided that the missing mass M_X (invariant mass of the two quarks) and $|Q|$ is much smaller than the c.m.s. energy $\sqrt{s}$. In this region the leading contribution to the cross section comes from the Pomeron exchange. At Born level and in the framework of QCD the Pomeron is represented by a pair of gluons in the color singlet state. In all our figures the bottom line represents a quark which could be a gluon as well. The only thing we need is a source which radiates off soft gluons. As we will describe later, our simple two-gluon exchange will be substituted by the proton structure function. This is the only adequate model for a Pomeron in the framework of QCD. Phrased in terms of the proton structure function, at Born level the gluonic part of the proton structure function is represented by a pair of gluons. Considering studies addressing the two-gluon exchange [21], it may seem that phenomenologically the two-gluon exchange does not satisfy all properties of a soft Pomeron, but as we already stressed, we intend to work consistently inside the framework of QCD, and at least in LLA this seems to be the correct procedure. In the same sense we do not need to consider how the gluons couple to the quarks inside the proton in detail. This again is a question of calculating the proton structure function which cannot be done without some phenomenological input.

Figure 7, now, shows all the diagrams which have to be taken into account. Gauge invariance requires a set of diagrams which includes all permutations of the photon and the two-gluon lines. Diagrams with crossed gluon lines were not explicitly shown in Fig. 7, instead each single diagram represents the sum of two diagrams with and without crossed gluon lines. We do this because summing the crossed and uncrossed diagram (s-channel and u-channel contributions) results in the approximate cancellation of the real part of these two diagrams. Only the imaginary part is left. The momentum u which is transferred along the two gluons was already introduced in Sec. II. For simplicity we set u^2 which is the momentum transfer t equal to zero. This assumption is realistic, since the proton's form factor decreases strongly with increasing t. In the following discussion we further assume that the two gluons couple to a quark instead of the proton in the lower part of the diagram.

Since our approach is based on LLA we concentrate on the region of integration over $|l_t^2|$ (see Fig. 7) which yields some log in $|\bar{Q}_0^2|$. This requires the strong ordering of the transverse momenta (for notation see Fig. 7):

$$|Q^2| \gg |k_t^2| m \gg |l_t^2| \gg |u_t^2| \approx 0 . \quad (3.1)$$

The α_l component of the momentum l (we use Sudakov variables: $l = \alpha_l Q' + \beta_l p + l_t$) is fixed by taking the pole

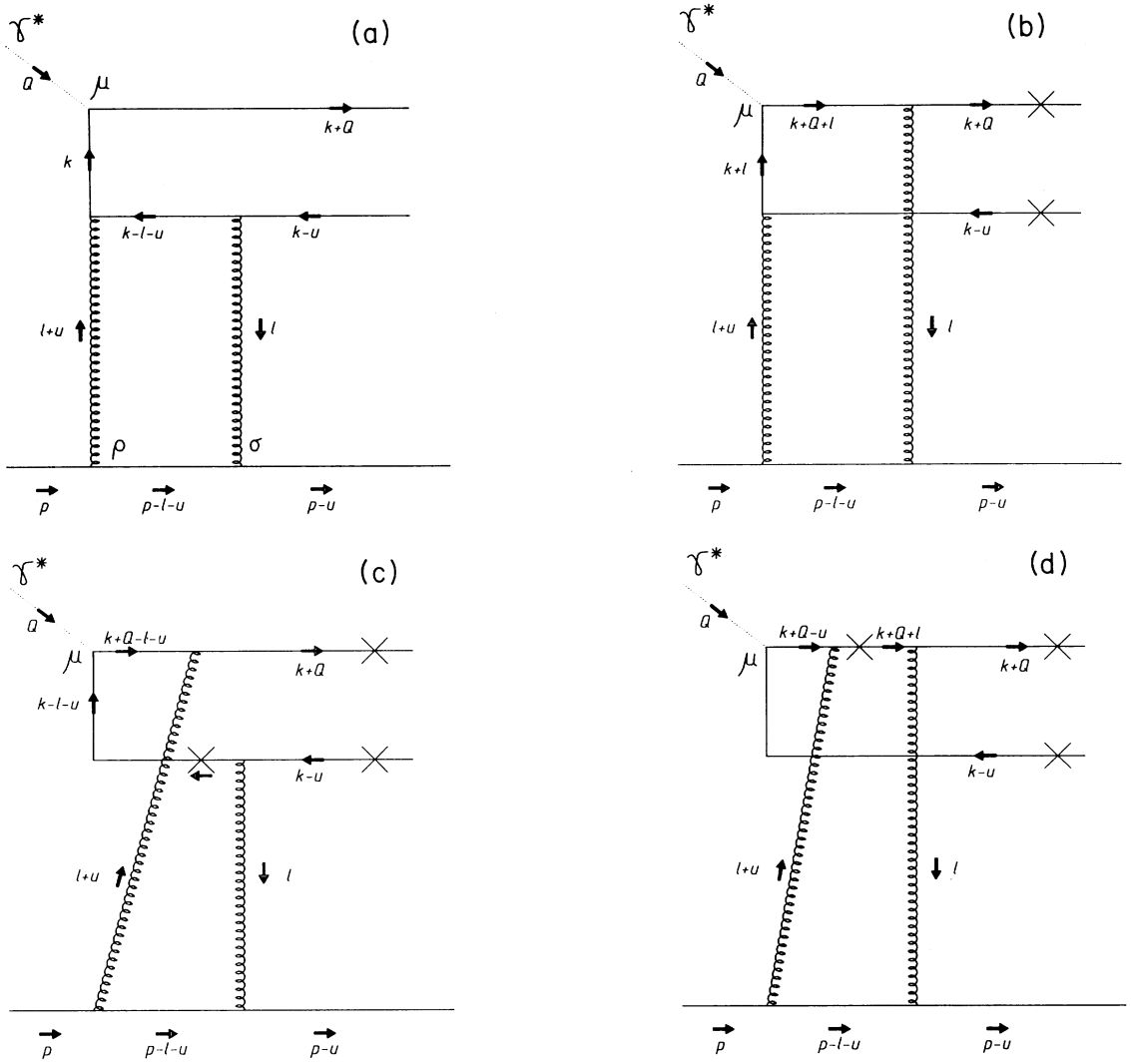

FIG. 7. Complete set of diagrams which contribute to the two-quark production at Born level.

of the propagator $p-u-l$, whereas α_u and α_k are fixed using the mass-shell condition of the final states with the momenta $p-u$ and $k-u$. The third mass-shell condition (momentum $k+Q$) serves to fix β_k.

We, now, come back to the point where we need the crossing of the gluons (crossing in the t channel, Fig. 8). As we already mentioned taking the sum of the crossed and uncrossed diagram is equivalent to the sum of the s-channel and u-channel contributions. Due to the positive signature of our diagrams (color singlet state) we know that the real part cancels out, at least in the leading-order neglecting terms proportional to $\frac{M_X^2}{s}$. The remaining imaginary part of each diagram in Fig. 7 is given by the imaginary part of the propagator $k-l-u$ and $k+Q+l$, respectively. In order to evaluate this imaginary part we just have to substitute a δ function for each propagator. It is important to remark that each δ function is accompanied by one π and not 2π as usually appears while taking the pole of some propagator. We can say that due to the smallness of the momentum u

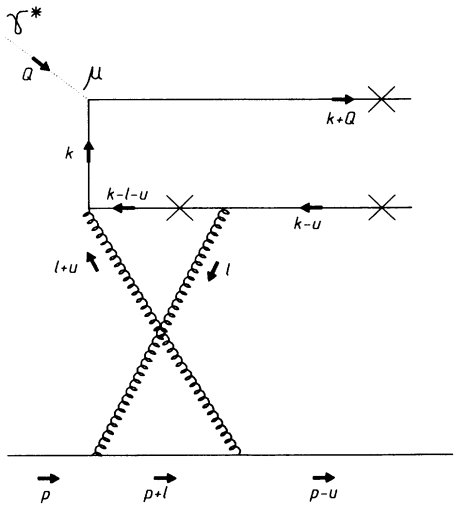

FIG. 8. u-channel contribution corresponding to the diagrams in Fig. 7.

the amplitude is approximately equal to the half of its discontinuity.

We have already mentioned that in our approach we set t equal to zero. It follows that u_t and α_u are zero, too. This means that the momentum u has only one component along p ($u = \beta_u p$). β_u can be expressed in terms of the missing mass M_X and $|Q^2|$:

$$M_X^2 = (Q+u)^2 \Rightarrow \beta_u = \frac{M_X^2 + |Q^2|}{s} . \tag{3.2}$$

We now give all kinematical relations which we have discussed so far:

$$\begin{aligned} \alpha_l &= \frac{l_t^2}{s} , \\ \alpha_u &= \frac{u_t^2}{s} = 0 , \\ \alpha_k &= \frac{k_t^2}{(\beta_u - \beta_k)s} , \\ \text{(a) } \beta_l &= \frac{l_t^2 - 2(l_t, k_t)}{\alpha_k s} , \\ \text{(b) } \beta_l &= 0 , \\ \beta_k &= x , \\ \beta_u &= \frac{M_X^2}{s} + x , \\ u^2 &= u_t^2 = t = 0 . \end{aligned} \tag{3.3}$$

For β_t we have two different results: (a) belongs to Figs. 7(a) and 7(c) and (b) to Figs. 7(b) and 7(d). From Eqs. (3.3) it is clear together with Eq. (3.1) that all α variables are strongly ordered:

$$1 \gg |\alpha_k| \gg |\alpha_l| \gg |\alpha_u| = 0 . \tag{3.4}$$

We would like to illustrate this in the case of $|\alpha_k|$ and $|\alpha_l|$. There are two reasons why these two variables are strongly ordered. The first is that we assumed $|k_t^2| \gg |l_t^2|$ and the second one is the smallness of x and β_u: $\beta_u - x = M_X^2/s \ll 1$. So, even if l_t is not much smaller than k_t, α_l is small compared to α_k and we are allowed to neglect it. This neglection we have already used while calculating β_l in Eqs. (3.3).

After having clarified the kinematical situation we proceed with the calculation of the lower part of the diagrams in Fig. 7. In each diagram the pair of gluons is radiated by a very fast moving quark.[3] The gluons are sufficiently soft ($M_x^2/s \ll 1$) and the emission could be understood as virtual bremsstrahlung. In the language of Feynman rules this means that we can use the eikonal approximation. For example,

$$\bar{u}(p-u)\gamma^\sigma(\hat{p} - \hat{l} - \hat{u})\gamma^\rho u(p) \approx 4p^\sigma p^\rho \bar{u}(p)u(p) . \tag{3.5}$$

All other contributions turn to be beyond the leading order that we are interested in. We see that the gluons are polarized along p. So far we have not specified the gauge. If we assumed the Feynman gauge, the polarization vector p^σ of each gluon would be directly transmitted to the top of the diagram. With this p vector we could go on calculating the upper fermion line, but instead we prefer to use a trick which will help us to reduce the number of diagrams which actually have to be calculated. Figure 9 shows that we can isolate out of Figs. 7(a) and 7(c) a gauge-invariant substructure. Gauge invariance is guaranteed because the quark with the momentum $k-l-u$ is on mass shell [$(k-l-u)^2 = 0$]. Let us call the upper part of Fig. 9, where the gluon is coupled to M^ρ. Then

$$(l+u)_\rho M^\rho = 0 \Rightarrow p_\rho M^\rho = -\frac{l_{t\rho}}{\beta_l + \beta_u} M^\rho . \tag{3.6}$$

We neglected α_l as well as u_t. Equation (3.6) is generally known as Ward identity. In Appendix A we show how this result is reached by summing explicitly the two diagrams in Fig. 9. Using the polarization $-l_{t\rho}/(\beta_l + \beta_u)$

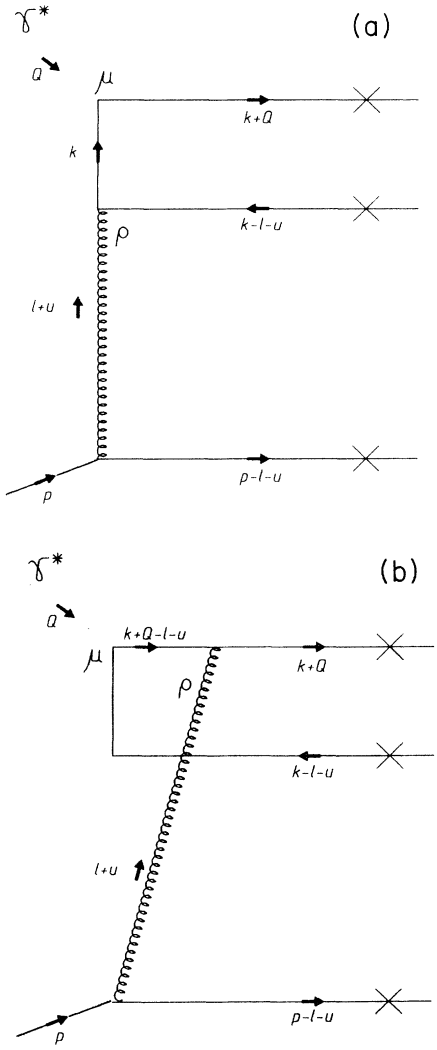

FIG. 9. Dipole emission in the t channel.

[3]We work in the Breit frame.

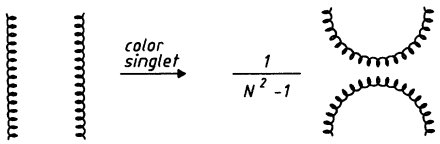

FIG. 10. Graphical representation of the color singlet projector.

instead of p^ρ allows to neglect the diagram in Fig. 9(b) because its contribution is proportional to $(l_t, k_t)/s$.

A further possibility usually used to calculate the Altarelli-Parisi splitting function is the use of the light-cone gauge with Q' as gauge vector $(A \cdot Q' = 0)$. In this gauge the propagator looks as follows (k is any vector):

$$\frac{-id^{\mu\nu}(k)}{k^2} \tag{3.7}$$

with

$$d^{\mu\nu}(k) = g^{\mu\nu} - \frac{k^\mu Q'^\nu + Q'^\mu k^\nu}{(k, Q')} . \tag{3.8}$$

Multiplying $d^{\mu\nu}(k)$ by p_μ directly yields $-k_t^\nu/\beta_k$ where we neglected $\alpha_k Q'^\nu$. For the right gluon in Fig. 7 which carries the momentum l we keep p polarization.

We finally come to the conclusion that we only need to evaluate the diagrams in Figs. 7(a) and 7(b), whereas those in Figs. 7(c) and 7(d) do not contribute provided we use as polarization vector for the left gluon $-l_t^\rho/(\beta_l + \beta_u)$.

We go on with the evaluation of the upper fermion line in Figs. 7(a) and 7(b):

$$-\bar{u}(k+Q)\gamma_{t_\mu}\frac{\hat{k}}{k^2}\frac{\hat{l}_t}{\beta_l+\beta_u}(\hat{k}-\hat{l}-\hat{u})\hat{p}v(u-k)\frac{\pi}{\alpha_k s} ,$$

$$\bar{u}(k+Q)\hat{p}(\hat{k}+\hat{Q}+\hat{l})\gamma_{t_\mu}\frac{\hat{k}+\hat{l}}{(k+l)^2}\frac{\hat{l}_t}{\beta_l+\beta_u}v(u-k)\frac{\pi}{s} . \tag{3.9}$$

Since we consider only transverse polarized photons, we introduced in Eq. (3.9) γ_{t_μ} instead of γ_μ for the photon vertex. The factor $\pi/\alpha_k s$ and π/s in Eq. (3.9) is the result of integrating the δ functions which have to be introduced in order to calculate the imaginary part of the amplitude as explained above.

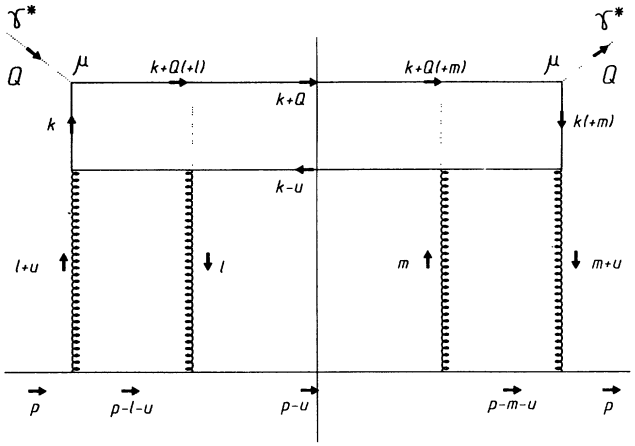

FIG. 11. The squared amplitude of two-quark production (Born level).

Both expressions in Eq. (3.9) have to be explained to the order l_t^2/k_t^2, for we would like to extract the log over l_t^2. The details how to proceed is given in Appendix A. The result for both expressions in Eq. (3.9) is

$$2z(1-z)\bar{u}(k+Q)\gamma_{t_\mu}v(u-k)\frac{\pi l_t^2}{\beta_u k_t^2} . \tag{3.10}$$

The variable z is defined as $z = \beta_k/\beta_u = x/\beta_u$.

Next, we would like to evaluate the color coefficient of the diagrams in Fig. 7. This is easy to do, for the pair of gluons is assumed to make up a color singlet state. Figure 10 shows how this looks graphically. We only have to deal with a gluon loop which is attached to a fermion line. The result is simply

$$\frac{C_F}{N^2-1} = \frac{1}{2N} . \tag{3.11}$$

We would like to conclude this subsection with the complete expression for the cross section of photon diffractive dissociation at Born level (see Fig. 11):

$$\left.\frac{\beta_u d\sigma}{d\beta_u dt}\right|_{t=0} = \sum_F \frac{4\pi^2\alpha_{\rm em}e_F^2}{|Q^2|}\frac{x}{\beta_u}\int_{|Q_0^2|}^{|Q^2|}\frac{d|k_t^2|}{k_t^4}\frac{\alpha_s^2}{16}\frac{8}{N}z^2(1-z)^2\left(4C_F\int_{|Q_0^2|}^{|k_t^2|}\frac{d|l_t^2|}{|l_t^2|}\frac{\alpha_s}{4\pi}\right)^2 . \tag{3.12}$$

We remind the reader that a factor $\frac{1}{4}$ is due to averaging over the polarizations of the incoming quark and transverse photon. $|Q_0^2|$ is as usual the initial virtuality of the quark in the proton. We already introduced the value $|\bar{Q}_0^2|$ as lower cutoff for the transverse momentum squared (k_t^2) in Sec. II. It should be large enough to justify perturbative QCD and to give room for some evolution from $|Q_0^2|$ to $|\bar{Q}_0^2|$.

As was noted before, expression (3.12) could be derived from the result of Nikolaev and Zakharov [6] by passing to LLA. The main modification that we made, was to introduce the lower cutoff $|\bar{Q}_0^2|$ for the transverse momentum in the quark loop, and we neglected all quark masses. The difference becomes visible in the asymptotic region of a large missing mass M_X. In this region only small values of the transverse momentum contribute. From Eq. (3.12) we deduce an asymptotic spectrum of the type

$$\frac{d\sigma}{dt\,dM_X^2} \approx \frac{Q^4}{|\bar{Q}_0^2|M_X^8} . \tag{3.13}$$

This equation shows that our leading log result is strongly suppressed at large M_X. In this region the Pomeron acts as a pointlike particle. This behavior is better described by the formula of Nikolaev and Zakharov:

$$\frac{d\sigma}{dtdM_X^2} \approx \frac{1}{m_f^2 M_X^4} . \tag{3.14}$$

Such a type of spectrum is typical for a pointlike particle similar to a gluon or photon. There is only one quark exchange in the t channel (see, for example, Fig. 11). We would like to stress that Eq. (3.14) does not contradict our result, it is just outside the region where LLA is applicable. But, it is only a very small fraction of the total cross section.

B. Photon diffractive dissociation into three jets

On the way to some complete expression for the cross section of diffractive dissociation we have to investigate the case when besides the two quark jets one additional gluon jet is emitted. Before we look at all the diagrams which may contribute we have to specify in which gauge we would like to work. In contrast to Ryskin [5] we use the light-cone gauge with Q' as gauge vector $[(A,Q')=0]$. We think that in this gauge it is more convenient to calculate the diagrams in the kinematical region where β_u could be of the same order as x. This gauge can also be used to derive the Altarelli-Parisi splitting functions in a similar way as was done by Dokshitzer, Dyakohov, and Troyan (DDT) [20].

We have already introduced the corresponding propagator [see (3.7) and (3.8)] which is

$$\frac{-id^{\mu\nu}(r)}{r^2} \tag{3.15}$$

with

$$d^{\mu\nu}(r) = g^{\mu\nu} - \frac{r^\mu Q'^\nu + Q'^\mu r^\nu}{(r,Q')} . \tag{3.16}$$

r can be any momentum. Apart from the propagator we need the polarization vector of a real gluon, i.e., a gluon on a mass shell:

$$\epsilon^\mu(r) = \epsilon_t^\mu(r) - \frac{[r_t,\epsilon_t(r)]}{(r,Q')}Q'^\mu . \tag{3.17}$$

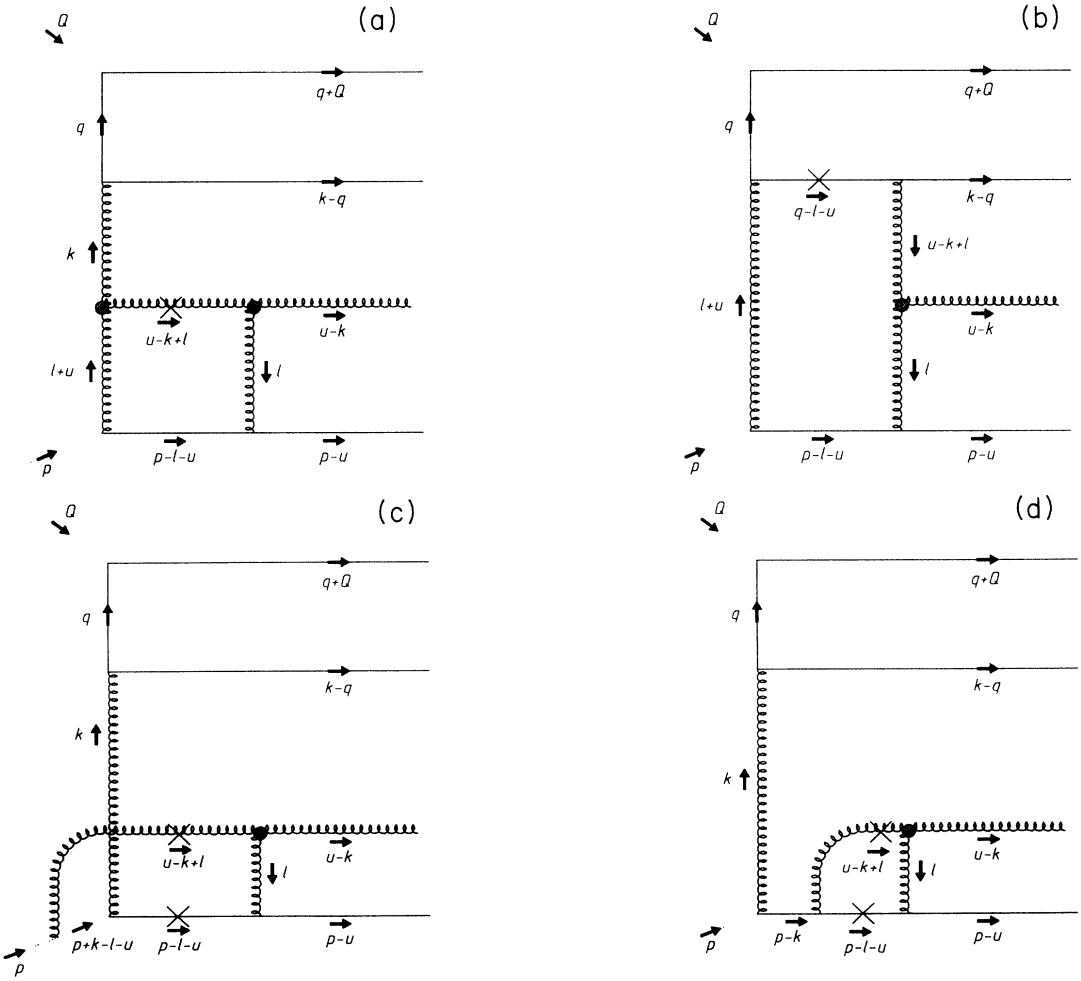

FIG. 12. The first set of diagrams for the three-jet production (two quarks and one gluon).

$\epsilon_t(r)$ denotes a vector in the transverse momentum plane which has the following properties:

$$[\epsilon_t(r), \epsilon_t(r)] = -1 ,$$
$$\sum_{\text{Pol}} \epsilon_t^{\mu}(r)\epsilon_t^{\nu}(r) = -g_t^{\mu\nu} . \tag{3.18}$$

Since the transverse plane is two dimensional we only need two basic polarization vectors. When we sum over the polarizations as in Eq. (3.18) we actually sum over these basic polarization vectors. In practice we only need the second relation in (3.18).

The kinematical situation is similar to that in the previous subsection. We have strong ordering in the transverse momenta and the α components:

$$|Q^2| \gg |q_t| \gg |k_t^2| \gg |l_t^2| \gg |u_t^2| = 0 ,$$
$$1 \gg |\alpha_q| \gg |\alpha_k| \gg |\alpha_l| \gg |\alpha_u| = 0 . \tag{3.19}$$

As a lower cutoff for $|k_t^2|$ we will assume $|\bar{Q}_0^2|$, whereas for $|l_t^2|$ we have the usual $|Q_0^2|$. The mass-shell conditions (see Fig. 12) including the poles of the propagator $p-l-u$, $k-l-u$ as well as $q-l-u$ lead to the following kinematical relations:

$$\alpha_q = \frac{q_t^2}{(\beta_k - \beta_q)s} ,$$
$$\alpha_k = \frac{k_t^2}{(\beta_u - \beta_k)s} ,$$
$$\alpha_l = \frac{l_t^2}{s} ,$$
$$\alpha_u = \frac{u_t^2}{s} = 0 ,$$
$$\beta_q = x , \tag{3.20}$$
$$\text{(a)}\ \beta_l = \frac{l_t^2 - 2(l_t, k_t)}{\alpha_k s} ,$$
$$\text{(b)}\ \beta_l = 0 ,$$
$$\beta_u = \frac{M_X^2}{s} + x ,$$
$$u^2 = u_t^2 = t = 0 .$$

Here again we used the fact that the imaginary part of our diagrams dominate over the real part. The variable β_k, now, has to be integrated. It ranges from β_u down to x.

We are interested in the asymptotic behavior $(1/k_t^4)\ln(|Q^2|/k_t^2)$ where the logarithm is a result of the $|q^2|$ integration. In order to extract these contributions each amplitude has to be proportional to q_t^1/q_t^2. The numerator originates from the gluon-quark vertex and the denominator from the quark propagator. In analogy to the subsection before we are going to extract the logarithmic contribution over l_t^2 from all diagrams.

The variety of diagrams which may contribute is quite large, now. But the specific choice of the gauge and the fact that we are only interested in terms proportional to l_t^2 reduce their number. The gauge that we chose allows to neglect diagrams with real gluon emission from their top, i.e., emission from the upper fermion line, whereas emission from the bottom gives some contribution. The light-cone gauge with p as gauge vector $[(p, A) = 0]$ has the opposite effect (see [5]). There, the emission from the bottom can be neglected.

We conclude that it is enough to calculate the set of diagrams given in Figs. 12 and 14. One example of di-

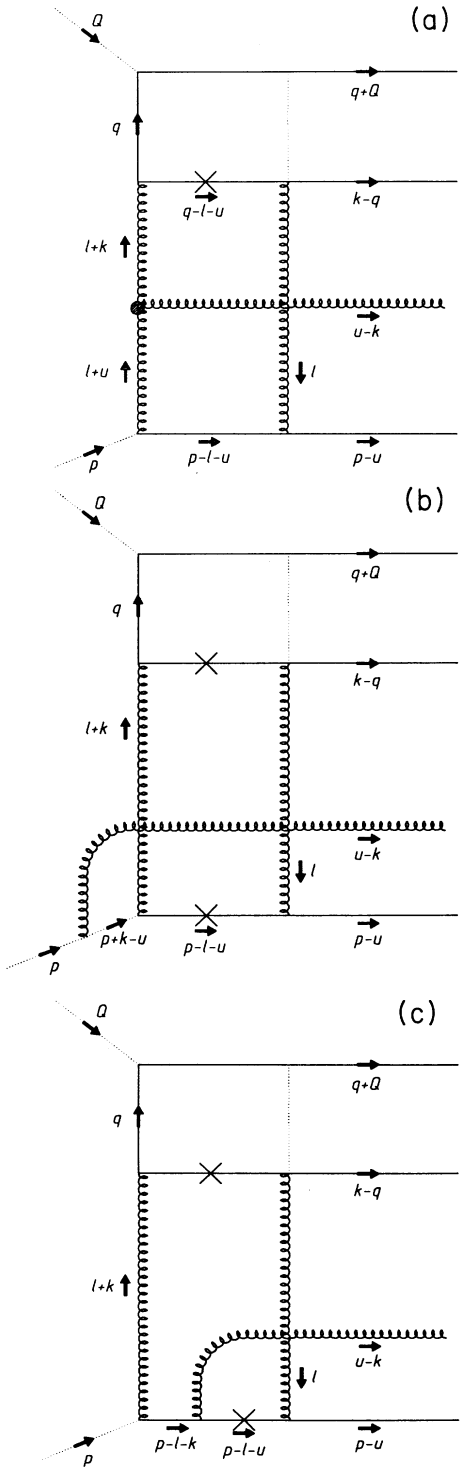

FIG. 13. The second set of diagrams for the three-jet production.

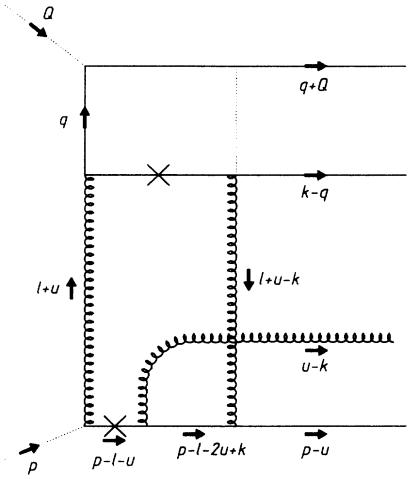

FIG. 14. One example of diagrams which does not contribute in the leading log approximation. The diagram is the same as in (c) but the kinematic is different.

agrams which do not contribute is shown in Fig. 14. It yields a contribution which is proportional to l_t^1/l_t^4. The details of the calculation we leave for Appendix A and present here only the final answer and some general remarks.

We divided up the complete set of diagrams into two groups, Figs. 12 and 14. The difference between them is, roughly speaking, the fact that in Fig. 12 we have an interaction in the final state between the gluon and the bottom quark whereas in Fig. 13 the common property is the interaction between the quark pair at the top and the bottom quark. One could object that the diagram in Fig. 12(b) does not perfectly fit into this group but the final answer suggests to put it there because, then, the result of all diagrams in Fig. 12 is the same as in Fig. 13.

The polarization vector of all the gluons which are emitted from the bottom line are aligned along the momentum p. If we multiply now the vector p^ρ by $d^{\rho\mu}(l+u)$ we get $-\frac{l_t^2}{\beta_l+\beta_u}$. For the second lower t-channel gluon with momentum l it turns out to be more convenient to keep the p polarization. This is possible, since the lines on the right and on the left to the point where this gluon is attached are on mass shell except in Fig. 13(b). The local gauge invariance allows us to change the gauge. In Fig. 13(b) we have this possibility, too, but now, at the top where the right t-channel gluon couples to the quark line. The quarks on both sides of the vertex are on mass-shell again. The numerator of the propagator $l+u-k$ can be changed from

$$\frac{Q'^\nu(k_t-l_t)^\mu}{(\beta_l+\beta_u-\beta_k)(p,Q')} \tag{3.21}$$

to

$$\frac{Q'^\nu p^\mu}{p,Q'}\,. \tag{3.22}$$

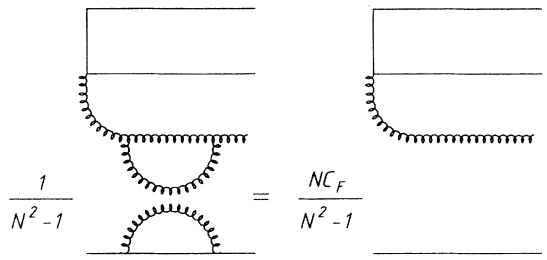

FIG. 15. Color coefficient of the three-jet production.

The t-channel gluons on which we focus at the moment (so-called Coulomb gluons) have a specific property: due to the fact that they couple to two particles on mass shell their β components turn out to be small, i.e., they are very soft. The smallness of the β component allows us to use the approximate form (3.21) instead of $d^{\nu\mu}(l+u-k)$.

Another important property of these soft gluons is the fact that they feel the total charge of the quark-antiquark pair and not its substructure. This may be illustrated with the help of the following example [see Fig. 14(a)]:

$$\frac{(\hat{q}-\hat{l}-\hat{k})\hat{p}v(k-q)}{\alpha_q s} \approx v(k-q)\,. \tag{3.23}$$

The $\alpha_q s$ in the denominator is the residue of the propagator $q-l-k$ in connection with the integration over β_l. Equation (3.23) only holds if we demand to have a logarithmic integration over q_t^2.[4] Taking into account the second quark with a similar approximation as in Eq. (3.23) the color of both quarks add up to the color of the left gluon. The approximation which was used in Eq. (3.23) we already know from the gluon emission at the bottom, it is the eikonal approximation. This type of approximation is intimately related to the classical current emission (see [5,16]).

The previous discussion and its application gives a great simplification in the calculation of all diagrams in Figs. 12 and 14. The total color structure becomes easy to handle and can be reduced to the structure in Fig. 15. Due to the color singlet state of the lower gluon pair the color coefficient in Fig. 12(b) is the negative of the color coefficient in Fig. 12(a). The color coefficient of Figs. 13(c) and 13(d) add up to give again the same as in Fig. 12(a) and in a similar way all diagrams of Fig. 13 can be normalized to Fig. 13(a).

The amplitude which finally represents the sum of all diagrams in Figs. 12 and 13 is proportional to

[4]For the sake of completeness we should add a minus to Eq. (3.23) due to the direction of the fermion line (incoming).

$$-eg_s^3\frac{\pi}{\beta_u k_t^2}\frac{N}{N^2-1}T^a_{ij}\bar{u}(q+Q)\gamma_{t_\mu}\frac{\hat{q}}{q^2}\hat{\epsilon}_t(u-k)v(k-q)2(1-z)^2\left(2+\frac{1}{z}\right)4C_F\int_{Q_0^2}^{k^2}\frac{d|l+t^2|}{|l_t^2|}\frac{\alpha_s}{4\pi}\,. \tag{3.24}$$

z is defined as $\frac{\beta_k}{\beta_u}$. The indices a, i, and j are the color indices of the gluon, quark, and antiquark. Over the colors of the incoming quark we averaged.

To complete the discussion we give the cross section of the three-jet event (see Fig. 16)

$$\left.\frac{\beta_u d\sigma}{d\beta_u dt}\right|_{t=0}=\sum_F\frac{4\pi^2\alpha_{\rm em}e_F^2}{|Q^2|}\int_{\frac{x}{\beta_u}}^1\frac{dz}{z}\frac{x}{\beta_u}\int_{|Q_0^2|}^{|Q^2|}\frac{d|k_t^2|}{k_t^4}\frac{\alpha_s^2}{16}\int_{|k_t^2|}^{|Q^2|}\frac{d|q_t^2|}{|q_t^2|}\frac{\alpha_s}{4\pi}$$
$$\times\left\{\Phi_G^F\left(\frac{x}{z\beta_u}\right)\Phi_P^G(z)+\Phi_F^F\left(\frac{x}{\beta_u z}\right)\Phi_P^F(z)\right\}\left(4C_F\int_{|Q_0^2|}^{|k_t^2|}\frac{d|l_t^2|}{|l_t^2|}\frac{\alpha_s}{4\pi}\right)^2 \tag{3.25}$$

and define two Pomeron splitting functions, the first one describes the Pomeron splitting into two gluons and the second one the splitting into two quarks:

$$\Phi_P^G(z)=\frac{2N^2}{N^2-1}4z(1-z)^3\left(2+\frac{1}{z}\right)^2\,,$$
$$\Phi_P^F(z)=\frac{1}{2N}16z^2(1-z)^2\,. \tag{3.26}$$

Φ_G^F and Φ_F^F are the usual Altarelli-Parisi splitting functions. The first one describes the production of two quarks by a gluon and the second one describes the emission of a real gluon by a quark. It is easy to see that the square of expression (3.24) leads to the first term in the square brackets of expression (3.25). It corresponds to Fig. 16(a). The integral over z was originally the integral over β_k. The evaluation of the second term in the square brackets of (3.25) follows the same strategy as was used before. That is, extracting terms proportional to $\frac{q_t^1}{q_t^2}$ leads to the usual Altarelli-Parisi splitting function convoluted with the Pomeron splitting function derived in the previous section.

We have to give a warning at this place. It is not possible to use expression (3.25) to make realistic computation on three-jet events. This can only be done with the help of Monte Carlo simulations. We emphasize that expression (3.25) is only one step on the way to a complete expression of diffractive dissociation cross section.

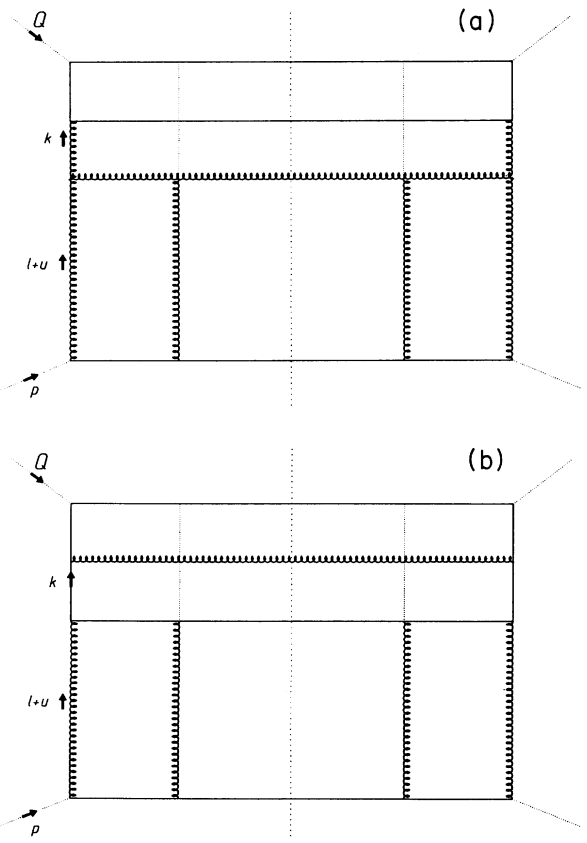

FIG. 16. The squared amplitude of the three-jet production.

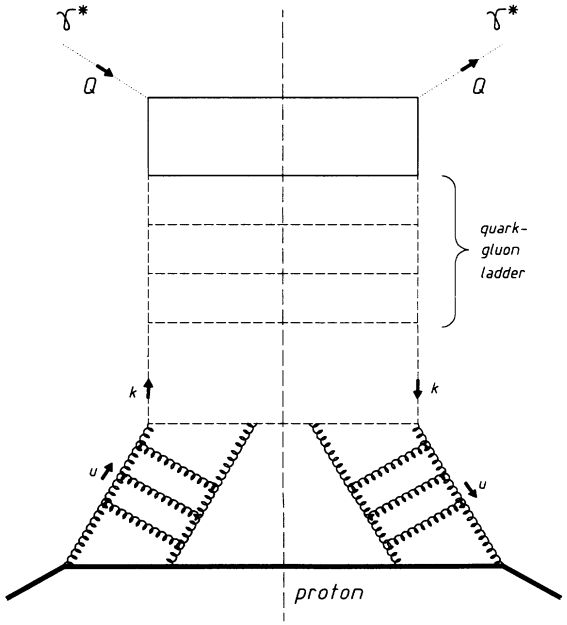

FIG. 17. Generalization to the emission of any number of jets.

IV. GENERALIZATION TO MULTIJET PRODUCTION AND THE PROTON STRUCTURE FUNCTION

Since we are interested in the total cross section of diffractive dissociation, we have to go beyond the three-jet production and take into account the emission of an arbitrary number of jets (see Fig. 17). When we talk about the total cross section we usually think about its hard contribution. As we have already explained in Secs. II B and II C, to be sure not to enter the soft region where perturbative QCD is invalid we have to introduce some cutoff $|\bar{Q}_0^2|$. Our hope is that, nevertheless, the hard contribution is the main contributions. This question could by checked by fitting $|\bar{Q}_0^2|$ in comparison to some phenomenological soft triple Pomeron model. If $|\bar{Q}_0^2|$ turns out to be rather large, this would indicate that, indeed, most of the cross section could be traced back to some hard interactions. We must emphasize at this point that there is, as usual in hadron physics, some nonperturbative input to our process. But, this nonperturbative input is hidden in the proton structure function that we will introduce below. The use of the proton structure function improves our simple model of the Pomeron just being made up of a pair of gluons in the color singlet state. The structure function D_p^G enters our calculations via the following substitution:

$$4C_F \int_{|Q_0^2|}^{|k_t^2|} \frac{d|l_t^2|}{|l_t^2|} \frac{\alpha_s}{4\pi} \to \beta_u D_p^G(\beta_u, |k_t^2|, |Q_0^2|) \, . \tag{4.1}$$

This procedure is well defined in the sense of $|Q^2|$-evolved (leading log) structure functions. The nonperturbative contribution comes in at the same low scale $|Q_0^2|$ in the shape of the initial x distribution. The proton form factor G_p^{2G} in our master formula (2.18) was introduced by hand.

As far as the production of jets is concerned the answer is quite simple if only the higher twist $\frac{1}{k_t^4}$ contribution dominates. Then we can proceed as in Sec. III B and each extra emitted gluon or quark results in a logarithmic integration over its transverse momentum together with the corresponding Altarelli-Parisi splitting function. Taking Eq. (3.25) we just have to substitute the Altarelli-Parisi splitting function by the parton density function, for example Φ_F^F by D_F^F. This procedure yields

$$\left.\frac{\beta_u d\sigma}{d\beta_u dt}\right|_{t=0} = \sum_F \frac{4\pi^2 \alpha_{\rm em} e_F^2}{|Q^2|} \int_{\frac{x}{\beta_u}}^1 \frac{dz}{z} \frac{x}{\beta_u} \int_{|Q_0^2|}^{|Q^2|} \frac{d|k_t^2|}{k_t^4} \frac{\alpha_s^2}{16}$$
$$\times \left[\Phi_P^G(z) D_G^F\left(\frac{x}{z\beta_u}, |Q^2|, |k_t^2|\right) + \Phi_P^F(z) D_F^F\left(\frac{x}{\beta_u z}, |Q^2|, |k_t^2|\right) \right] [\beta_u D_p^G(\beta_u, |k_t^2|, |Q_0^2|)]^2 \, . \tag{4.2}$$

V. CONCLUSIONS

The basic result of this paper is the evaluation of the photon diffractive dissociation cross section over a wide range of the missing mass M_X beyond the triple Regge region. The corresponding diffractive dissociation structure function obeys the GLAP-evolution equation with an additional inhomogeneous term and zero initial condition. This inhomogeneous term contains two new functions which we have introduced as Pomeron splitting functions Φ_P^F and Φ_P^G [see Eq. (2.19)]. The final result will be valid in the region

$$0 \le \frac{M_X^2}{s} \ll 1 \, . \tag{5.1}$$

The evolution starts at some initial scale $|\bar{Q}_0^2|$ which has to be understood as the lower cutoff in the transverse jet momenta. This cutoff should be large enough in order to stay outside the confinement, but much smaller than $|Q^2|$ in order to allow enough room for evolution.

We have studied our result in terms of the Pomeron structure function and have found that factorization into a Pomeron flux factor and a Pomeron structure function does not hold exactly, but as a rough approximation. How good this approximate factorization is has to be examined numerically. Assuming factorization one can use the functions Φ_P^F and Φ_P^G after having them normalized with respect to the energy sum as initial condition for the evolution of the Pomeron structure function. The gluon momentum fraction of the Pomeron, then, is about (100–1.9n_F)% (n_F is the number of flavors) which demonstrates the gluon dominance in the Pomeron.

We would like to make some comments on the difference to the earlier preprint version of this paper. In the current version we omitted the discussion of the so-called higher twist term in the master equation (2.18) and the AGK-cutting rules. Both questions will be discussed by Bartels and one of us (M.W.) in a paper that will be published soon. We would like to stress that the calculations presented in this paper are correct, but consider only the leading twist case. The answer to the question of the AGK-cutting rules originate in a deeper understanding of what they mean. We hope that our results will help to explain diffractive dissociation events at HERA.

ACKNOWLEDGMENTS

We would like to thank J. Bartels who initiated one of us (M.W.) to work on this subject as well as N. N. Nikolaev, M. G. Ryskin, and G. Ingelman for fruitful discussions. One of us (E.L.) is also grateful to the DESY Theory Division for its kind hospitality.

APPENDIX A

In this appendix we present some more details about the calculation in Sec. III A starting with Fig. 9. By summing the two diagrams in Fig. 7 we will show in an explicit way that the polarization vector p^ρ can be substituted by $-\frac{l_t^\rho}{\beta_l + \beta_u}$:

$$\bar{u}(k+Q)\gamma_t^\mu \frac{\hat{k}}{k^2}\hat{p}v(k-l-u)+\bar{u}(k+Q)\hat{p}\frac{\hat{k}+\hat{Q}-\hat{l}-\hat{u}}{(k+Q-l-u)^2}\gamma_t^\mu v(k-l-u)\,. \tag{A1}$$

The denominator $(k+Q-l-u)^2$ is equal to $-(\beta_l+\beta_u)s$. Each s in the denominator has to be compensated by some s in the numerator. This can be achieved only by taking the leading contribution of the expression $\bar{u}(k+Q)\hat{p}(\hat{k}+\hat{Q}-\hat{l}-\hat{u})$ which is $s\bar{u}(k+Q)$. Furthermore, we can change $\hat{p}v(k-l-u)$ into $\frac{\hat{k}-\hat{l}_t}{\beta_l+\beta_u}v(k-l-u)$ after the multiplication and the division by $\beta_l+\beta_u$. We then see the cancellation of the leading terms in (A1) which results in

$$\bar{u}(k+Q)\gamma_t^\mu\frac{\hat{k}}{k^2}\left(-\frac{\hat{l}_t}{\beta_l+\beta_u}\right)v(k-l-u)\,. \tag{A2}$$

This is exactly what we wanted to prove.

We proceed with Eq. (3.9) of Sec. III A and recall the first expression:

$$-\bar{u}(k+Q)\gamma_t^\mu\frac{\hat{k}}{k^2}\frac{\hat{l}_t}{\beta_l+\beta_u}(\hat{k}-\hat{l}-\hat{u})\hat{p}v(k-u)\frac{\pi}{\alpha_k s}\,. \tag{A3}$$

In the first step we extract all terms of the order l_t^2 which are the leading terms. The terms of the order l_t^1 cancel out. It is enough to expand each of the factors $\hat{k}-\hat{l}-\hat{u}$ and $\frac{1}{\beta_l+\beta_u}$ to the first order in l_t. We should remind here that β_l depends on l_t:

$$\beta_l=\frac{l_t^2-2(l_t,k_t)}{\alpha_k s}\,. \tag{A4}$$

In the expression $(\hat{k}-\hat{l}-\hat{u})\hat{p}\beta_l$ does not contribute, since $\beta_l\hat{p}\hat{p}$ is equal to zero. The factor $\frac{1}{\beta_l+\beta_u}$ leads to $\frac{1}{\beta_u}\frac{2(l_t,k_t)}{\beta_u\alpha_k s}$. So we have

$$-\bar{u}(k+Q)\gamma_t^\mu\frac{\hat{k}}{k^2}\frac{\hat{l}_t}{\beta_u}\left[\frac{2(l_t,k_t)}{\beta_u\alpha_k s}(\hat{k}-\hat{u})-\hat{l}_t\right]\hat{p}v(k-u)\frac{\pi}{\alpha_k s}\,. \tag{A5}$$

Integration over the azimuth angle of l_t yields

$$-\bar{u}(k+Q)\gamma_t^\mu\frac{\hat{k}}{k^2}\left[\frac{\hat{k}_t}{\beta_u^2\alpha_k s}(\hat{k}-\hat{u})\hat{p}-\frac{\hat{p}}{\beta_u}\right]v(k-u)\frac{\pi l_t^2}{\alpha_k s}\,. \tag{A6}$$

Now and for further transformations we frequently use the following identity:

$$\bar{u}(k+Q)\gamma_t^\mu\hat{Q}'\approx 0\,. \tag{A7}$$

This is easily proved by taking the square of the expression (A7):

$$\mathrm{Sp}\{\gamma_t^\mu(\hat{k}+\hat{Q})\gamma_{t_\mu}\hat{Q}'\cdots\}\approx 0\,. \tag{A8}$$

Since β_k is equal to x we find that $\gamma_t^\mu(\hat{k}+\hat{Q})\gamma_{t_\mu}$ approximately coincides with $\hat{Q}'$ where we neglect terms proportional to $\frac{k_t^2}{s}$. Remembering the fact that $u=\beta_u p$ we can write (A6) as

$$-\frac{\pi l_t^2}{\beta_u k^2}\bar{u}(k+Q)\gamma_t^\mu\left[\frac{\beta_k\hat{p}\hat{k}_t\hat{k}\hat{p}+k_t^2\hat{k}\hat{p}}{\beta_u\alpha_k^2 s^2}-\frac{\hat{k}\hat{p}}{\alpha_k s}\right]v(k-u)\,. \tag{A9}$$

The next simplification comes from the identity $\hat{k}\hat{p}v(k-u)=\alpha_k s v(k-u)$ where, again, we make use of the relation $u=\beta_u p$ and $p^2=0$. From Eqs. (3.3) we get $\beta_u\alpha_k s=\frac{k_t^2}{1-z}$ with $z=\frac{\beta_k}{\beta_u}$, and Eq. (A9) can be transformed into

$$-\frac{\pi l_t^2}{\beta_u k^2}\bar{u}(k+Q)\gamma_t^\mu\left[z\frac{\hat{p}\hat{k}_t}{\alpha_k s}-z\right]v(k-u)\,. \tag{A10}$$

For further reduction we use the following chain of relations: $\hat{p}\hat{k}_t v(k-u)=\hat{p}(\hat{k}-\alpha_k\hat{Q}')v(k-u)=-\hat{p}\alpha_k\hat{Q}'v(k-u)=(-\alpha_k s+\alpha_k\hat{Q}'\hat{p})v(k-u)$, and with the help of Eq. (A7) we finally find

$$\frac{\pi l_t^2}{\beta_u k^2}2z\bar{u}(k+Q)\gamma_t^\mu v(k-u)\,. \tag{A11}$$

Next, we evaluate the second expression of Eq. (3.9):

$$\bar{u}(k+Q)\hat{p}(\hat{k}+\hat{Q}+\hat{l})\gamma_{t_\mu}\frac{\hat{k}+\hat{l}}{(k+l)^2}\frac{\hat{l}_t}{\beta_l+\beta_u}v(u-k)\frac{\pi}{s}\,. \tag{A12}$$

The s in the denominator can only be compensated by the leading term of $\bar{u}(k+Q)\hat{p}(\hat{k}+\hat{Q}+\hat{l})$ which is $s\bar{u}(k+Q)$. β_l is zero in this case. The expansion of the propagator gives

$$\frac{1}{(k+l_t)^2}\approx\frac{1}{k^2}-\frac{2(l_t,k_t)}{k^4}\,. \tag{A13}$$

Extracting the terms of second order in l_t from the total expression (A12) leads to

$$\frac{\pi}{\beta_u k^2}\bar{u}(k+Q)\gamma_{t_\mu}\left(-\frac{\hat{k}\hat{l}_t 2(l_t,k_t)}{k^2}+l_t^2\right)v(u-k)\,. \tag{A14}$$

Integration over the azimuth angle of l_t yields

$$\frac{\pi l_t^2}{\beta_u k^2}\bar{u}(k+Q)\gamma_{t_\mu}\left(-\frac{\hat{k}\hat{k}_t}{k^2}+1\right)v(u-k)\,. \tag{A15}$$

Using Eq. (A7) and the relation $k^2=\frac{k_t^2}{1-z}$ finally results

in the same expression as in Eq. (A10). This means that the sum of all diagrams in Fig. 7, i.e., the final answer of this section, is equal to expression (A11) multiplied by two:

$$\frac{\pi l_t^2}{\beta_u k^2} 4z\bar{u}(k+Q)\gamma_t^\mu v(k-u) \ . \tag{A16}$$

APPENDIX B

In this section we come back to the calculation of the diagrams in Figs. 12 and 14. These diagrams describe the process of diffractive dissociation including the emission of one gluon.

We start with Fig. 13(a) and take out the right gluon vertex:

$$\Gamma_{\mu\nu\rho}(l+u-k,-l,k-u) = g_{\mu\nu}(-2l-u+k)_\rho + g_{\nu\rho}(k-u+l)_\mu + g_{\rho\mu}(l+2u-2k)_\nu \ . \tag{B1}$$

The gluons to the left with the momentum $l+u-k$ and to the right with the momentum $u-k$ are on mass shell, so that we can use the polarization vector $\epsilon^\mu(l+u-k)$ and $\epsilon^\rho(u-k)$ for real gluons. From below we have p^ν as polarization vector:

$$\begin{aligned}\epsilon^\mu(l+u-k)\epsilon^\rho(u-k)\Gamma_{\mu\nu\rho}p^\nu = {} & (p,\epsilon(l+u-k))(-2l,\epsilon(u-k)) + (2l,\epsilon(l+u-k))(p,\epsilon(u-k)) \\ & -\alpha_k s(\epsilon(l+u-k),\epsilon(u-k)) \ .\end{aligned} \tag{B2}$$

This expression yields

$$2\frac{(l_t-k_t,\epsilon_t(l+u-k))}{\beta_l+\beta_u-\beta_k}(l_t,\epsilon_t(u-k)) + 2(l_t,\epsilon_t(l+u-k))\frac{(k_t,\epsilon_t(u-k))}{\beta_u-\beta_k} - \alpha_k s(\epsilon_t(l+u-k),\epsilon_t(u-k)) \ . \tag{B3}$$

Next, we take the left gluon vertex

$$\Gamma_{\mu\nu\rho}(-l-u+k,-k,l+u) = g_{\mu\nu}(-2k+l+u)_\rho + g_{\nu\rho}(l+u+k)_\mu + g_{\rho\mu}(-2l-2u+k)_\nu \ . \tag{B4}$$

We will use the polarization vector $\epsilon^\nu(k)$ even for an off mass-shell gluon. This is possible, since Q'^ν applied to the upper quark loop does not contribute, at least not at the desired order. From below we now have $-\frac{l_t^\rho}{\beta_l+\beta_u}$:

$$\begin{aligned}\epsilon^\nu(k)\epsilon^\mu(l+u-k)\Gamma_{\mu\nu\rho}\left(-\frac{l_t^\rho}{\beta_l+\beta_u}\right) = {} & (\epsilon(k),\epsilon(l+u-k))\frac{2(l_t,k_t)-l_t^2}{\beta_l+\beta_u} - 2\frac{(l_t,\epsilon(k))}{\beta_l+\beta_u}(l+u,\epsilon(l+u-k)) \\ & +2\frac{(l_t,\epsilon(l+u-k))}{\beta_l+\beta_u}(l+u,\epsilon(k)) \ .\end{aligned} \tag{B5}$$

This expression is evaluated to be

$$(\epsilon_t(k),\epsilon_t(l+u-k))\frac{2(l_t,k_t)-l_t^2}{\beta_l+\beta_u} - 2(l_t,\epsilon_t(k))\frac{(l_t-k_t,\epsilon_t(l+u-k))}{\beta_l+\beta_u-\beta_k} - 2\frac{(l_t,\epsilon_t(l+u-k))}{\beta_k}(k_t,\epsilon(k)) \ . \tag{B6}$$

Next, we have to multiply (B6) and (B3) and sum over the polarization of the gluon with momentum $l+u-k$:

$$\begin{aligned}
& 4\frac{(l_t-k_t,\epsilon_t(k))}{\beta_l+\beta_u-\beta_k}(l_t,\epsilon_t(u-k))\frac{(l_t,k_t)-\frac{1}{2}l_t^2}{\beta_l+\beta_u} + 4(l_t,\epsilon_t(k))\frac{(l_t-k_t)^2(l_t,\epsilon_t(u-k))}{(\beta_l+\beta_u-\beta_k)^2} \\
& -4\frac{(l_t,l_t-k_t)}{\beta_l+\beta_u-\beta_k}\frac{(k_t,\epsilon_t(k))}{\beta_k}(l_t,\epsilon_t(u-k)) + 4(l_t,\epsilon_t(k))\frac{(k_t,\epsilon_t(u-k))}{\beta_u-\beta_k}\frac{(l_t,k_t)-\frac{1}{2}l_t^2}{\beta_l+\beta_u} \\
& +4(l_t,\epsilon_t(k))\frac{(l_t,l_t-k_t)}{\beta_l+\beta_u-\beta_k}\frac{(k_t,\epsilon_t(u-k))}{\beta_u-\beta_k} - 4l_t^2\frac{(k_t,\epsilon_t(k))}{\beta_k}\frac{(k_t,\epsilon_t(u-k))}{\beta_u-\beta_k} \\
& -2\alpha_k s(\epsilon_t(k),\epsilon_t(u-k))\frac{(l_t,k_t)-\frac{1}{2}l_t^2}{\beta_l+\beta_u} - 2\alpha_k s(l_t,\epsilon_t(k))\frac{(l_t-k_t,\epsilon_t(u-k))}{\beta_l-\beta_u-\beta_k} \\
& +2\alpha_k s\frac{(l_t,\epsilon_t(u-k))}{\beta_k}(k_t,\epsilon_t(k)) \ .
\end{aligned} \tag{B7}$$

From this expression we would like to extract the second order in l_t. While we do this we have to take into account that β_l depends on l_t:

$$\begin{aligned}\frac{1}{\beta_1+\beta_u} &\approx \frac{1}{\beta_u} + \frac{2(l_t,k_t)}{\beta_u^2\alpha_k s} \ , \\ \frac{1}{\beta_l+\beta_u-\beta_k} &\approx \frac{1}{\beta_u-\beta_k} + \frac{2(l_t,k_t)}{(\beta_u-\beta_k)^2\alpha_k s} \ .\end{aligned} \tag{B8}$$

So we get

$$-4\frac{(k_t,\epsilon_t(k))}{\beta_u-\beta_k}(l_t,\epsilon_t(u-k))\frac{(l_t,k_t)}{\beta_u}+4(l_t,\epsilon_t(k))\frac{k_t^2}{(\beta_u-\beta_k)^2}(l_t,\epsilon_t(u-k))$$

$$+4\frac{(l_t,k_t)}{\beta_u-\beta_k}\frac{(k_t,\epsilon_t(k))}{\beta_k}(l_t,\epsilon_t(u-k))+4(l_t,\epsilon_t(k))\frac{(k_t,\epsilon_t(u-k))}{\beta_u-\beta_k}\frac{(l_t,k_t)}{\beta_u}$$
$$-4(l_t,\epsilon_t(k))\frac{(l_t,k_t)}{\beta_u-\beta_k}\frac{(k_t,\epsilon_t(u-k))}{\beta_u-\beta_k}-4l_t^2\frac{(k_t,\epsilon_t(k))}{\beta_k}\frac{(k_t,\epsilon_t(u-k))}{\beta_u-\beta_k}$$
$$+\alpha_k s(\epsilon_t(k),\epsilon_t(u-k))\frac{l_t^2}{\beta_u}-4(\epsilon_t(k),\epsilon_t(u-k))\frac{(l_t,k_t)^2}{\beta_u^2}$$
$$-2\alpha_k s(l_t,\epsilon_t(k))\frac{(l_t,\epsilon(u-k))}{\beta_u-\beta_k}+4(l_t,\epsilon_t(k))\frac{(k_t,\epsilon_t(u-k))}{\beta_u-\beta_k}\frac{(l_t,k_t)}{\beta_u-\beta_k}\,. \tag{B9}$$

Integration over the azimuth angle of l_t yields

$$-2\frac{(k_t,\epsilon_t(k))}{\beta_k}\frac{(k_t,\epsilon_t(u-k))}{\beta_u-\beta_k}l_t^2+2(\epsilon_t(k),\epsilon_t(u-k))\frac{k_t^2}{(\beta_u-\beta_k)^2}l_t^2$$
$$+\alpha_k s(\epsilon_t(k),\epsilon_t(u-k))\frac{l_t^2}{\beta_u}-2(\epsilon_t(k),\epsilon_t(u-k))\frac{k_t^2}{\beta_u}l_t^2-\alpha_k s(\epsilon_t(k),\epsilon_t(u-k))\frac{l_t^2}{\beta_u-\beta_k}\,. \tag{B10}$$

In the following equations we would like to include the residue of the β_l integration together with the corresponding π and the factor $\frac{1}{k^2}$ originating from the propagator. All this leads to an extra factor

$$\frac{\pi}{\alpha_k s}\frac{1}{k^2}\,. \tag{B11}$$

With $z=\frac{\beta_z}{\beta_u}$ and $\beta_u\alpha_k s=k^2$, we reduce the equation (B10):

$$\frac{\pi l_t^2}{\beta_u k^2}\left\{-\frac{2}{z(1-z)}\frac{(k_t,\epsilon_t(k))(k_t,\epsilon_t(u-k))}{k^2}+z\frac{3-2z}{1-z}(\epsilon_t(k),\epsilon_t(u-k))\right\}\,. \tag{B12}$$

The next diagrams which we will calculate are those in Figs. 12(c) and 12(d). The right gluon vertex is the same as in Fig. 12(a). Instead of the left gluon vertex we now have

$$-\frac{(k_t,\epsilon_t(k))}{\beta_k}\frac{(2p,\epsilon(1+u-k))}{\alpha_k s}l_t^2=2\frac{(l_t-k_t,\epsilon_t(l+u-k))}{(l_t-k_t)^2}l_t^2\frac{(k_t,\epsilon_t(k))}{\beta_k}\,. \tag{B13}$$

The $\alpha_k s$ comes from the propagator at the bottom line. In order to make expression (B13) comparable with Fig. 13(a) we multiplied by l_t^2. Later on we will divide all contributions by l_t^4 which corresponds to the two propagators with momentum $l+u$ and l in Fig. 13(a). In the further procedure we multiply expression (B13) by (B3) and sum over the polarization as before. Since expression (B13) is already of second order in l_t we only need to take the third term in Eq. (B3). The result is

$$2\frac{(k_t\epsilon_t(k))}{\beta_k}\alpha_k s l_t^2\frac{(k_t,\epsilon_t(u-k))}{k_t^2}\,. \tag{B14}$$

After multiplication by the factor (B11) we see that this result cancels the first term in expression (B12). Indeed, taking into account Fig. 13(d) the color coefficient adds up to give the same as in Fig. 13(a). So we are left with

$$\frac{\pi l_t^2}{\beta_u k^2}z\frac{3-2z}{1-z}(\epsilon_t(k),\epsilon_t(u-k))\,. \tag{B15}$$

The last diagram in the first group is the one in Fig. 12(b). We have already discussed in Sec. III B that the quark pair at the top of the diagram acts as a classical current with regard to the soft gluon with momentum $l+u-k$. One conclusion was that the β component equals zero. So we have

$$\beta_l+\beta_u=\beta_k\,. \tag{B16}$$

The gluon vertex is the same as in expression (B1), but from the top we now have $Q'^\mu/(p,Q')$ and from the bottom $-l_t^\nu/\beta_l$.

$$\frac{Q'^\mu}{(p,Q')}\left(-\frac{l_t^\nu}{\beta_l}\right)\Gamma_{\mu\nu\rho}(l+u-k,-l,k-u)\epsilon^\rho(u-k)$$
$$=-(\beta_k-\beta_u+\beta_l)\frac{(l_t,\epsilon_t(u-k))}{\beta_l}\,. \tag{B17}$$

Taking into account (B16) we find the simple result:

$$-2(l_t,\epsilon_t(u-k))\ . \tag{B18}$$

The left lower t-channel gluon which carries the momentum $l+u$ gives a contribution of the type

$$-\frac{(l_t,\epsilon_t(k))}{\beta_l+\beta_u}=-\frac{(l_t,\epsilon_t(k))}{\beta_k}\ . \tag{B19}$$

The denominator $(l+u-k)^2$ corresponding to the right upper t-channel gluon simply yields $(k_t-l_t)^2$. Together with (B18) and (B19) the final integration over the azimuth angle of l_t leads to

$$\frac{l_t^2}{\beta_u k^2}\frac{1}{z(1-z)}(\epsilon_t(k),\epsilon_t(u-k))\ . \tag{B20}$$

The residue of the β_l integration was canceled out by the emission vertex of the soft gluon with momentum $l+u-k$.[5] We only keep the π which has not been taken into account yet. Finally we have to be aware of the opposite sign with respect to Fig. 13(a) which is due to color.

We can now write down the final expression for the total sum of all diagrams in Fig. 12:

$$\frac{\pi l_t^2}{\beta_u k^2}\left(z\frac{3-2z}{1-z}-\frac{1}{z(1-z)}\right)(\epsilon_t(k),\epsilon_t(u-k))$$

$$=\frac{\pi l_t^2}{\beta_u k^2}(1-z)\left(2+\frac{1}{z}\right)(\epsilon_t(k),\epsilon_t(u-k))\ . \tag{B21}$$

Our next task is the calculation of the diagrams in Fig. 13. The gluon vertex in Fig. 14(a) is

$$\Gamma_{\mu\nu\rho}(-l-k,l+u,k-u)=g_{\mu\nu}(-2l-u+k)_\rho+g_{\nu\rho}(k-u+l)_\mu+g_{\rho\mu}(l+2u-2k)_\nu\ . \tag{B22}$$

The procedure is similar to that before in the case of Fig. 13(a). For the gluon with momentum $l+k$ we use the polarization vector $\epsilon^\mu(l+k)$. From below we have as usual $-\frac{l_t^\nu}{\beta_l+\beta_u}$, and we apply the polarization vector $\epsilon^\rho(u-k)$ which corresponds to the emitted real gluon:

$$\epsilon^\mu(l+k)\left(-\frac{l_t^\nu}{\beta_l+\beta_u}\right)\Gamma_{\mu\nu\rho}\epsilon^\rho(u-k)=-\frac{(l_t,\epsilon_t(l+k))}{\beta_l+\beta_u}2(l+u,\epsilon(u-k))+2(l+u,\epsilon(l+k))\frac{(l_t,\epsilon_t(u-k))}{\beta_l+\beta_u}$$
$$+(\epsilon(l+k),\epsilon(u-k))\frac{l_t^2+2(l_t,k_t)}{\beta_l+\beta_u}\ . \tag{B23}$$

Further evaluation gives

$$-2(l_t,\epsilon_t(l+k))\frac{(k_t,\epsilon_t(u-k))}{\beta_u-\beta_k}-2(l_t,k_t)\frac{(l_t+k_t,\epsilon_t(l+k))}{\beta_l+\beta_k}+(\epsilon_t(l+k),\epsilon_t(u-k))\frac{l_t^2+2(l_t,k_t)}{\beta_l+\beta_u}\ . \tag{B24}$$

In all diagrams of Fig. 13 we can set β_l equal to zero. Instead of $\frac{1}{\beta_l+\beta_u}$ we now have to expand the propagator $l+k$:

$$\frac{1}{(1+k)^2}=\frac{1}{l_t^2+2(l_t,k_t)+k^2}\approx\frac{1}{k^2}-\frac{2(l_t,k_t)}{k^4}\ . \tag{B25}$$

After combining this equation with expression (B24) and extracting all terms of second order in l_t we get

$$2\frac{(l_t,\epsilon_t(l+k))2(l_t,k_t)}{k^4}\frac{(k_t,\epsilon_t(u-k))}{\beta_u-\beta_k}-2\frac{(l_t,\epsilon_t(u-k))}{k^2}\frac{(l_t,\epsilon_t(l+k))}{\beta_k}$$
$$+2\frac{(l_t,\epsilon_t(u-k))2(l_t,k_t)}{k^4}\frac{(k_t,\epsilon_t(l+k))}{\beta_k}+\frac{(\epsilon_t(l+k),\epsilon_t(u-k))}{\beta_u k^2}l_t^2-2\frac{(\epsilon_t(l+k),\epsilon_t(u-k))}{k^4}\frac{2(l_t,k_t)^2}{\beta_u}\ . \tag{B26}$$

We still have to integrate over the azimuth angle of l_t which results in

$$\frac{\pi l_t^2}{\beta_u k^2}\left\{\frac{2}{z(1-z)}\frac{(k_t,\epsilon_t(l+k))(k_t,\epsilon_t(u-k))}{k^2}-(1-z)\left(2+\frac{1}{z}\right)(\epsilon_t(l+k),\epsilon_t(u-k))\right\}\ . \tag{B27}$$

where we included a π coming along with the β_l integration.

We now can already suspect what happens with the first term in Eq. (B27), if we add Figs. 14(b) and 14(c). It is canceled. The proof is quite easy to do. From Fig. 14(b) we have

$$-\frac{(l_t+k_t,\epsilon_t(l+k))}{\beta_l+\beta_k}2(p,\epsilon(u-k))\frac{l_t^2}{\alpha_k s}\frac{\pi}{(l+k)^2} \tag{B28}$$

which gives

$$-\frac{\pi l_t^2}{\beta_u k^2}\frac{2}{z(1-z)}\frac{(k_t,\epsilon_t(l+k))(k_t,\epsilon_t(u-k))}{k^2}\ . \tag{B29}$$

[5] Typical for classical current emission.

Figure 14(c) yields the same result, but the color coefficient is different. However, Figs. 14(b) and 14(c) sum up to give the same coefficient as in Fig. 14(a). The complete answer for all diagrams in Fig. 13 is

$$-\frac{\pi l_t^2}{\beta_u k^2}(1-z)\left(2+\frac{1}{z}\right)(\epsilon_t(l+k),\epsilon_t(u-k))\,. \quad \text{(B30)}$$

Expressions (B30) and (B21) can be viewed as identical, although they contain two different vectors $\epsilon_t(l+k)$ and $\epsilon_t(k)$. We introduced these vectors for technical reasons. To get rid of them we have to be aware that in the total amplitude there is a second pair of adjoint vectors $\epsilon_t^\mu(l+k)$ and $\epsilon_t^\mu(k)$ which transforms both of them into the projector on the vector component μ after summation over the polarization. So we can add up both expressions originating from Figs. 12 and 14 into one:

$$-\frac{\pi l_t^2}{\beta_u k^2}2(1-z)\left(2+\frac{1}{z}\right)(\epsilon_t(l+k),\epsilon_t(u-k))\,. \quad \text{(B31)}$$

We should mention that a more careful analysis shows that the sign due to the soft emitted gluon is compensated by the total color coefficient in Fig. 13, so that the sum of diagrams in Figs. 12 and 14 have the same sign and do not cancel out.

We conclude this subsection with one example of diagrams (see Fig. 14) which do not contribute. It is easy to check that this diagram is of third order in l_t, so beyond the LLA.

[1] A. B. Kaidalov and K. A. Ter-Martirosyan, Nucl. Phys. **B75**, 471 (1974).

[2] V. A. Abramovskii and R. G. Betman, Yad. Fiz. **49**, 1205 (1989) [Sov. J. Nucl. Phys. **49**, 747 (1989)].

[3] L. V. Gribov, E. M. Levin, and M. G. Ryskin, Phys. Rep. **100**, 1 (1983).

[4] J. Bartels and G. Ingelman, Phys. Lett. B **235**, 175 (1990).

[5] M. G. Ryskin, Sov. J. Nucl. Phys. **52**, 529 (1990).

[6] N. N. Nikolaev and B. G. Zakharov, Z. Phys. C **49**, 607 (1991); Phys. Lett. B **260**, 414 (1991); Z. Phys. C **53**, 331 (1992).

[7] G. Ingelman and P. E. Schlein, Phys. Lett. **152B**, 256 (1985).

[8] L. Frankfurt and M. Strikman, Phys. Rev. Lett. **63**, 1914 (1989).

[9] A. Donnachie and P. V. Landshoff, Nucl. Phys. **B244**, 322 (1984).

[10] E. L. Berger *et al.*, Nucl. Phys. **B286**, 704 (1987).

[11] G. Ingelman and K. Janson-Prytz, Phys. Lett. B **281**, 325 (1992).

[12] V. A. Abramovski, V. N. Gribov, and O. V. Kancheli, Sov. J. Nucl. Phys. **18**, 308 (1973).

[13] V. V. Sudakov, Zh. Eksp. Teor. Fiz. **30**, 187 (1956) [Sov. Phys. JETP **3**, 115 (1956)].

[14] V. N. Gribov and L. N. Lipatov, Yad. Fiz. **15**, 731 (1972) [Sov. J. Nucl. Phys. **15**, 438 (1972); L. N. Lipatov, *ibid.* **20**, 181 (1974); **20**, 94 (1975); Yu. L. Dokshitzer, Zh. Eksp. Teor. Fiz. **73**, 1216 (1977) [Sov. Phys. JETP **46**, 641 (1977)]; G. Altarelli and G. Parisi, Nucl. Phys. **B126**, 298 (1977).

[15] J. C. Collins, D. E. Soper, and G. Sterman, Nucl. Phys. **B261**, 104 (1985); **B308**, 833 (1988).

[16] A. Bassetto, M. Ciafaloni, and G. Marchesini, Phys. Rep. **100**, 201 (1983).

[17] J. Bartels and E. M. Levin, Nucl. Phys. **B387**, 617 (1992).

[18] J. Bartels, Phys. Lett. B **298**, 204 (1993).

[19] E. M. Levin, M. G. Ryskin, and A. G. Shuvaev, Nucl. Phys. **B387**, 589 (1992).

[20] Yu. L. Dokshitzer, D. I. Dyakonov, and S. I. Troyan, Phys. Rep. **58**, 269 (1980).

[21] D. G. Richards, Nucl. Phys. **B258**, 267 (1985).

[22] M. Wüsthoff, Diplomarbeit, University of Hamburg (unpublished).